# Investigation of Electroluminescence Degradation in Anthracene-based Organic Light-Emitting Devices

by

Qi Wang

A thesis
presented to the University of Waterloo
in fulfillment of the
thesis requirement for the degree of
Master of Applied Science
in
Electrical and Computer Engineering

Waterloo, Ontario, Canada, 2010

# AUTHOR'S DECLARATION

I hereby declare that I am the sole author of this thesis. This is a true copy of the thesis, including any required final revisions, as accepted by my examiners.

I understand that my thesis may be made electronically available to the public.

# Abstract

Organic light-emitting devices (OLEDs) have attracted significant attention because of their unique advantages for flat panel display applications. However, the relatively limited electroluminescence (EL) stability of blue emitting OLEDs continues to limit the commercialization of full color OLED displays. In most cases, the decrease in EL efficiency is also accompanied by a loss in blue color purity. Thus, the understanding of the degradation mechanisms of both the EL efficiency loss and color purity loss and the corresponding solutions to device degradation are required.

In this thesis, electrical aging mechanism in anthracene-based OLEDs is investigated by using a number of techniques, including delayed EL measurements. The studies reveal that electrical aging is associated with an increasing concentration of an intermolecular species with a weak characteristic luminescence at around 535 nm. This species is capable of trapping charges, and thus plays a role as an electron-hole recombination center with prolonged electrical driving. Weak green luminescence from this species leads to an increased green/blue emission ratio, and causes the color purity loss in aged devices. The results also suggest that this species is also efficient in dissipating excitation energy non-radiatively, hence is capable of quenching singlet excitons in anthracene-based OLEDs, contributing to the observed efficiency loss with electrical aging.

Moreover, the photo-stability of the organic/metal cathode interface in OLEDs is studied. Irradiating OLEDs by external illumination is found to result in a gradual increase in driving voltage and decrease in EL efficiency. This photo-induced degradation in device performance is found to be caused by changes at the organic/metal cathode interface that lead to a deterioration in electron injection. Evidence of photodegradation of the same interface, inherently, by device own EL, is also reported. The results uncover an important degradation mechanism in OLEDs and shed the light on a phenomenon that might limit the stability of other organic optoelectronic and photovoltaic devices.

## Acknowledgements

I would like to thank my supervisor, Prof. H. Aziz, for his continuous support, cultivation and encouragement in the last two years. I am grateful that I was led to a scientific world full of challenges, excitement and elegance. More importantly, besides the scientific knowledge I was more enlightened by his humbleness and integrity.

I also would like to thank Dr. Y. Luo. I have grasped so much knowledge and insight in both experimental and physical aspects from the helpful discussions with him in the last two years.

Last but not least, I would like to thank Prof. D. Ban and Prof. K. Karim for taking their time to review my thesis.

# Table of Contents

# List of Figures

# Chapter 1

# Introduction

Since last century, inorganic semiconductors such as Si or Ge began to lead as dominant materials in electronics from the previously prevailing metals. Meanwhile, the replacement of vacuum tube based electronics by solid state devices initiated a development of semiconductor microelectronics. Now, in the twenty-first century, a new revolution in electronics that has become possible due to the understanding and development of a new class of materials, called organic semiconductors. The enormous progress in this field has been achieved such as organic light emitting devices (OLEDs), organic filed effect transistors (OFETs) and organic solar cells (OSCs).

In terms of commercialization, OLEDs is the most successful among all the organic optoelectronic devices. Compared with liquid crystal display (CRT) and cathode ray tube (CRT), OLEDs have several advantages such as low cost, mechanical flexibility, lower power consumption, faster refresh rate, better contrast, wider viewing angle, lighter weight and ultra-thin size. Especially the advantages of the low cost and mechanical flexibility make OLEDs a very promising technology for flat-panel display in the near future.

## 1.1 Overview of OLEDs

There are a number of ways to generate light from a material as shown in figure 1.1 [1]. For instance, incandescence is the emission of light (visible electromagnetic radiation) from a hot body due to its temperature; bioluminescence is the production and emission of light by a living organism; chemoluminescence is the emission of light as the result of a chemical reaction; photoluminescence (PL) is a process in which a substance absorbs photons and then re-radiates photons; electroluminescence (EL) is an optical and electrical phenomenon in which a material emits light in response to an electric current passed through it. Particularly, OLEDs is based on the electroluminescence in organic materials, which is the effect that organic films subjected to an external electric field can emit light, converting electrical current to light without recourse of any intermediate energy forms.

**Figure 1.1: Different ways to generate light.**

In fact, EL in organic materials is not new. In the early 1950s, Bernanose *et al.* [2] at Université de Nancy first produced electroluminescence in organic materials by applying a high-voltage alternating current (AC) field to crystalline thin films of acridine orange and quinacrine. In 1960, researchers at Dow Chemical developed AC-driven electroluminescent cells using doped anthracene [3]. In 1963, Weiss *et al.* first reported high conductivity in iodine-doped oxidized polypyrrole [4]. They achieved a conductivity of 1S/cm. In 1977, Hideki Shirakawa et al. reported high conductivity in similarly oxidized and iodine-doped polyacetylene [5]. In 2000, Alan J. Heeger, Alan G. MacDiarmid and Hideki Shirakawa received the Nobel Prize in Chemistry for "The discovery and development of conductive organic polymers".

The first attempt to create a polymer LED was by Roger Partridge at the UK's National Physical Laboratory [6]. The first diode device was invented at Eastman Kodak by Ching W. Tang and Steven

Van Slyke in the 1980s [7]. This diode, giving rise to the term "OLED", used a novel two-layer structure with separate hole transporting and electron transporting layers such that recombination and light emission occurred in the middle of the organic layer. This resulted in a reduction in operating voltage and improvements in efficiency, and started the current era of OLED research and device production.

Normally the device structure of an OLED consists of a transparent anode, a hole transport layer (HTL), a light-emitting layer (EML), an electron transport layer (ETL) and a cathode, as shown in figure 1.2. When a forward bias is applied to an OLED, holes and electrons are injected from anode and cathode, and are transported through HTL and ETL, respectively, recombining to form exitons at EML. Finally the exitons either decay radiatively to emit photons or dissipate non-radiatively.

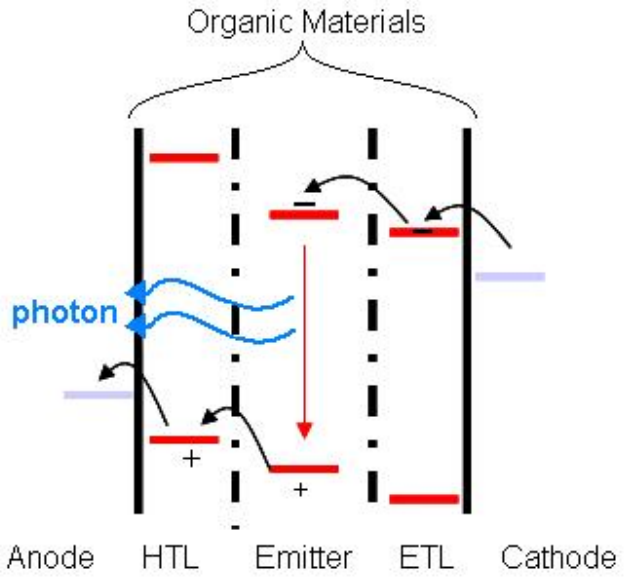


**Figure 1.2: Typical structure and energy level of OLEDs.**

Basically there are two types of OLEDs: those that are based on small molecules and those that employ polymers. Molecules commonly used in small molecule-based OLEDs (SMOLEDs) include organometallic chelates, fluorescent and phosphorescent dyes and conjugated dendrimers. The production of SMOLEDs usually involves thermal evaporation in vacuum which makes the cost of the production process more expensive. However, the vacuum deposition process enables the formation of well controlled, homogeneous organic films, and the construction of complex multi-layer structures, which are

the main reasons for achieving high efficiencies of SMOLEDs. On the other hand, polymers used in polymer LEDs (PLEDs) include derivatives of poly(p-phenylene vinylene) and polyfluorene. Substitution of side chains on the polymer backbone may determine the color of emitting light or the polymeric stability, as well as the solubility. Polymers are not suitable for vacuum deposition, but they can be processed from solution through spin coating. This method is more suited to forming large-area films than thermal evaporation. No vacuum is required, and the emissive materials can also be applied on the substrate by a technique derived from commercial inkjet printing [8]. However, the metal cathode typically needs to be deposited by thermal evaporation in vacuum.

Some typical organic small molecules and polymers that are widely used in OLEDs are shown in figure 1.3. The OLEDs in this thesis are based on small molecules.

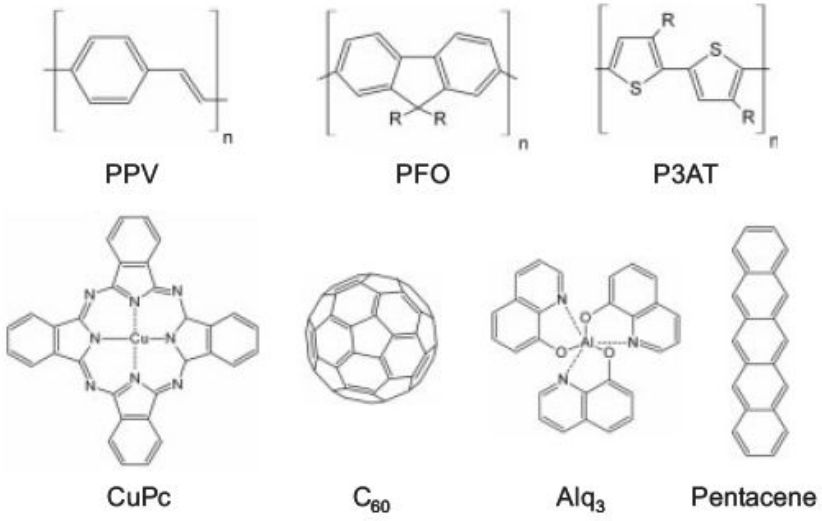


**Figure 1.3: Some organic molecules and polymers that widely used in OLEDs.**

The operation mechanisms of OLEDs include charge carrier injection, charge carrier transport and exciton formation and dissipation. These mechanisms will be introduced in detail in the following sections.

## 1.2 Charge Carrier Injection

In spite of extensive studies of OLEDs and its commercialized products, their operating mechanisms are not yet well understood. A better understanding of device physics is significant for improving the

existing devices. Energy level alignment at organic/electrode interfaces is one of the fundamental phenomena that strongly influence the performance of an OLED.

A simple model to discuss this problem is Mott-Schottky (MS) model [9], which is a well-known textbook model for inorganic semiconductor/metal contact. This model is illustrated in figure 1.4 [10] for an n-type semiconductor. When a neutral organic solid and a neutral metal are isolated, the energy levels of the two solids are aligned at the common vacuum level between the two solids. When the two solids make contact, the MS model assumes (1) a vacuum level alignment right at the interface region and (2) band bending in the space charge layer (SCL) to achieve the alignment of the bulk Fermi levels between them. In relation to band bending, the Fermi level alignment is a fundamental concept in the MS model. The thermal equilibrium state, in which Fermi level is constant everywhere in the system, is assumed to be achieved. Since the bulk Fermi level of a semiconductor coincides with that of the substrate metal, the built-in potential coincides with the difference in the work function between the electrode and the organic semiconducting solid.

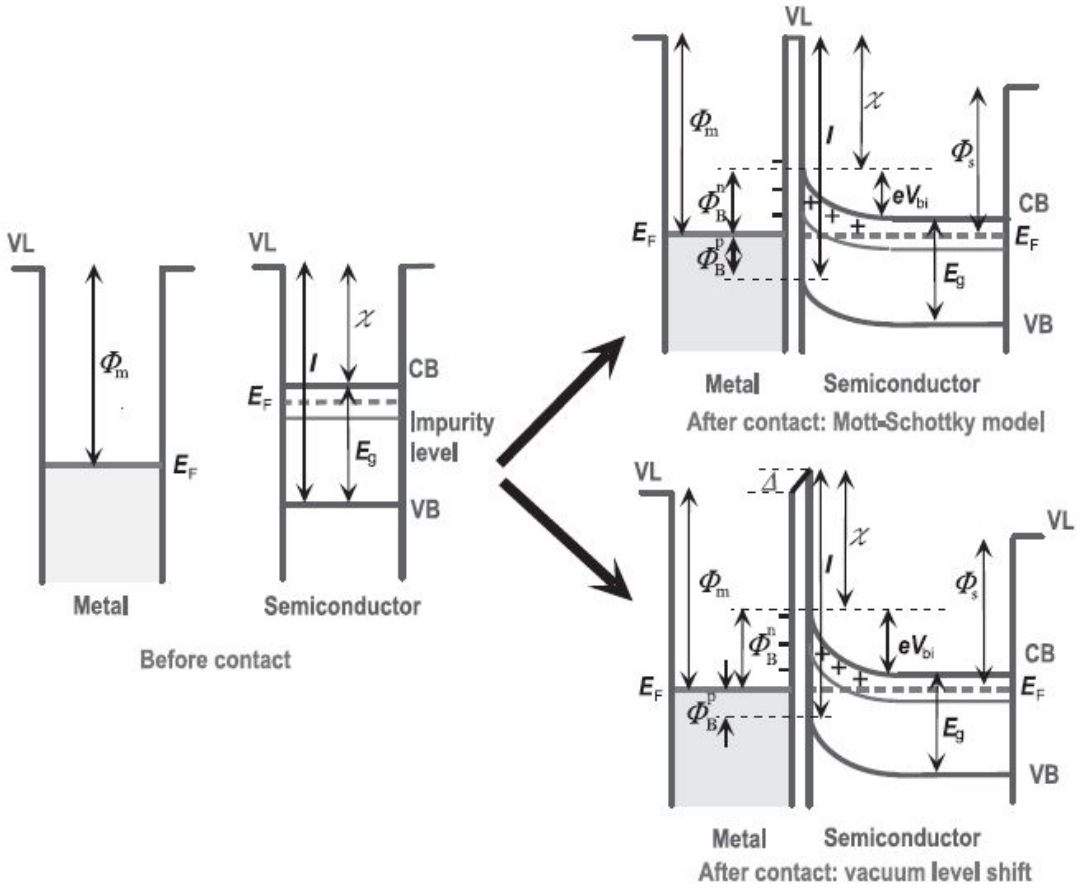


**Figure 1.4: Models for energy level alignment at organic semiconductor/metal contact.**

The above model is a very classical and simple one although it has been applied for a long time to discuss the interfaces of organic devices. As for the first assumption in MS model, studies revealed that vacuum level alignment does not occur in most organic/metal interfaces due to the formation of an interface dipole inducing vacuum level shift Δ [11]. The existence of Δ demonstrates that the barrier height estimated from the MS model has to be modified by the amount of Δ. Build-in voltage should be also modified by the same value.

Organic materials used as the active layer of electronic devices are usually called organic semiconductors, and their HOMO/LUMO gap is usually large (2~3 eV). Thus, the concentration of thermally excited carriers is extremely low, making them essentially non-conductive. So as for the second assumption in MS model, the band bending effect is usually neglected at insulator/organic interfaces.

In addition, Fermi level alignment is a critical issue. This scheme requires thermal equilibrium. Organic semiconductors are basically molecular solids where molecules are bound only by Van der Waals forces, and their properties such as wave function and charge density are fairly localized within each molecule. This means that the carrier exchange process between adjacent molecules is not effective in contrast to the case of inorganic semiconductors. Thus it is not obvious that the unbalance in the Fermi level can be compensated by the redistribution of carriers.

In the situation of organic electronic devices, band bending is closely related to the potential profile across the organic layer in devices with an applied external electric field. For example, in OLEDs, the electric field is often assumed to be constant and the potential is proportional to the position as shown in figure 1.5 [10]. Basically, a semiconductor with a sufficient carrier concentration can screen the external electric field. Polarization induced by an external field can exclude the penetration of the field deep into the inside of the semiconductor. This phenomenon is closely related to the concentration of mobile carriers and space charges.

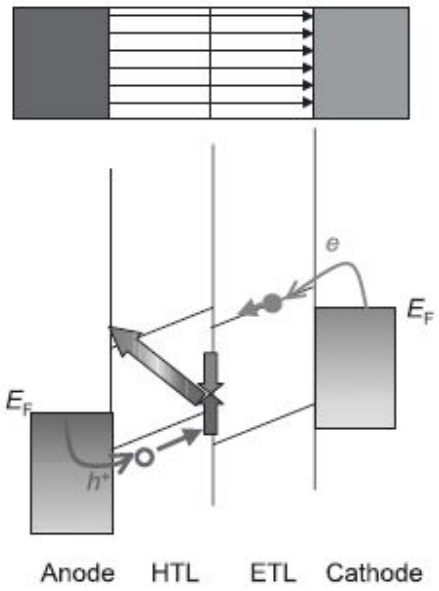


**Figure 1.5: Potential profiles in organic devices with no band bending.**

There are two proposed models for charge carrier injection from metal contact to organic layer, quantum mechanical tunneling of electrons through a triangular energy barrier and field-assisted

thermionic injection over the image force barrier. Their approximations for calculation and equations are shown in the figures below [12].

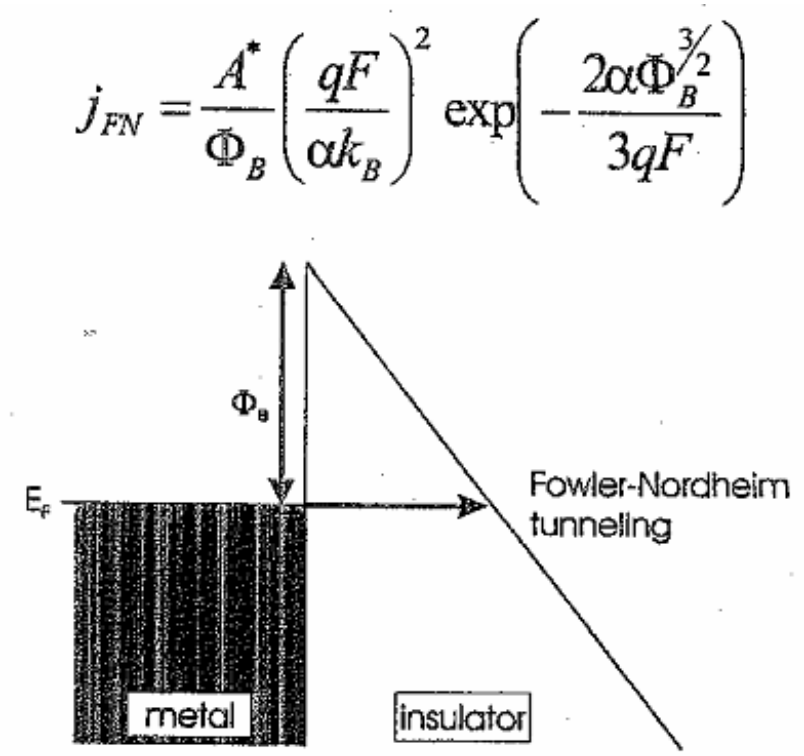


**Figure 1.6: Quantum mechanical tunneling of electrons through a triangular energy barrier.**

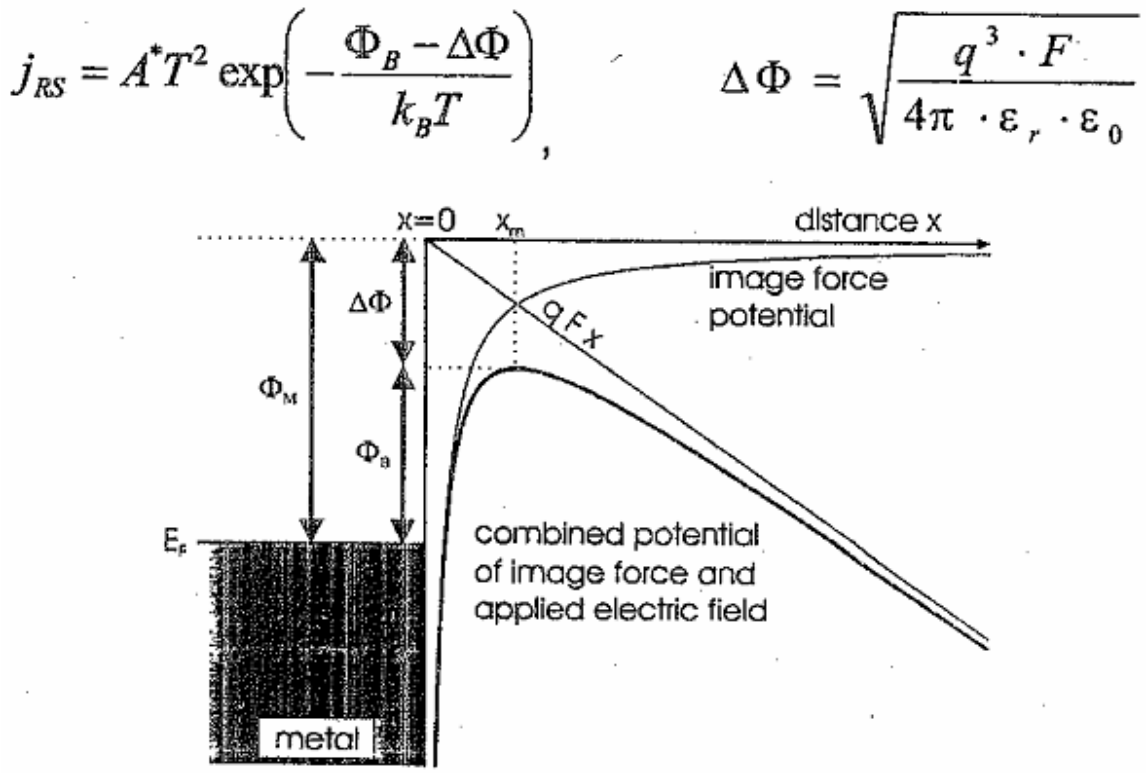


**Figure 1.7: Field-assisted thermionic injection over the image force barrier.**

## 1.3 Charge Carrier Transport

After the injection of the charge carriers from the anode and cathode, electrons and holes are transported across the organic layers. Compared with inorganic semiconductors, the transport mechanism in organic molecules is totally different. Organic molecules have a conjugated π-electron system being formed by the $p_z$-orbitals of $sp^2$-hybridized C-atoms in the molecules (see figure1.8 [13]). As compared to the σ-bonds forming the backbone of the molecules, the π-bonding is significantly weaker. Therefore, the lowest electronic excitations of conjugated molecules are the π-π*-transitions with an energy gap typically between 1.5 to 3eV.

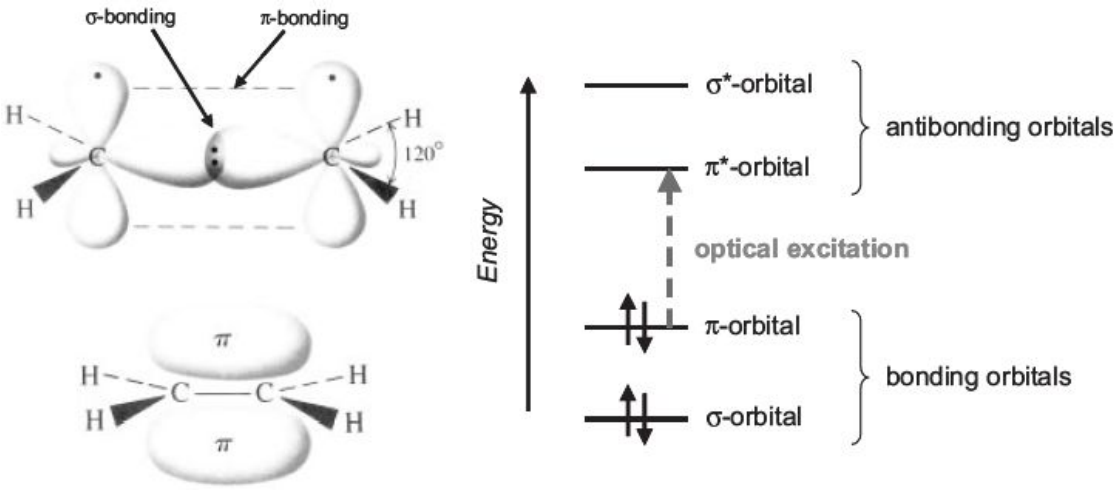


**Figure 1.8： Left: σ- and π-bonds in ethene, as an example for the simplest conjugated π-electron system. The right one shows the energy levels of a π-conjugated molecule. The lowest electronic excitation is between the bonding π-orbital and the anti-bonding π*-orbital.**

Compared to covalently bonded semiconductors like Si or GaAs, organic molecules are Van der Waals bonded, implying a much weaker intermolecular interaction. The consequences are the much weaker delocalization of electronic wavefunctions among neighboring molecules, which has direct implications for the charge carrier transport.

From inorganic crystals to disordered organic solids, one should consider locally varying polarization energies due to different molecular environments which lead to a Gaussian density of states (DOS) for the distribution of transport sites as shown in figure 1.9 [14]. The DOS function is described by:

$$\mathrm{DOS} = \frac{\mathrm{N_v}}{\sqrt{2\pi}\sigma} \exp[-(\frac{\mathrm{E}-\mathrm{E_0}}{\sqrt{2\pi}\sigma})^2]$$

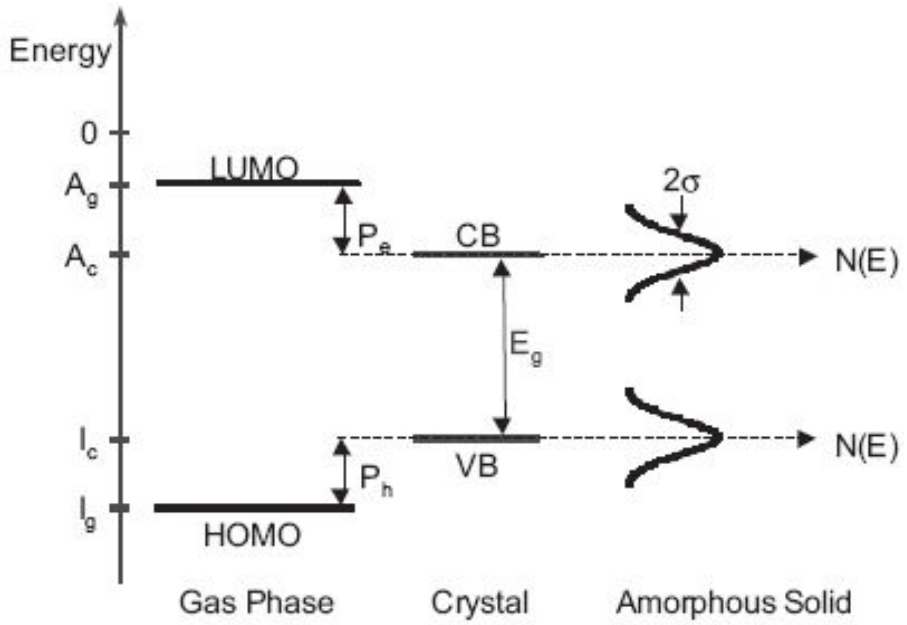


**Figure 1.9: Energy levels of an isolated molecule (left), a molecular crystal (middle) and an amorphous solid (right).**

Band transport is typically observed in highly purified inorganic semiconductor crystals. As a characteristic feature of band transport the mobility depends on temperature:

$\mu \propto T^{-n}$, where n is a positive integer.

However, since electronic delocalization is weak in organic semiconductors, hopping transport, as shown in figure 1.10, is the transport mechanism and the much lower mobility ($<10^{-3}$ $cm^2/Vs$) in hopping transport depends on both temperature and applied electric field described as below:

$\mu \propto \exp(-\Delta E/kT)\exp(\beta\sqrt{F}/kT)$

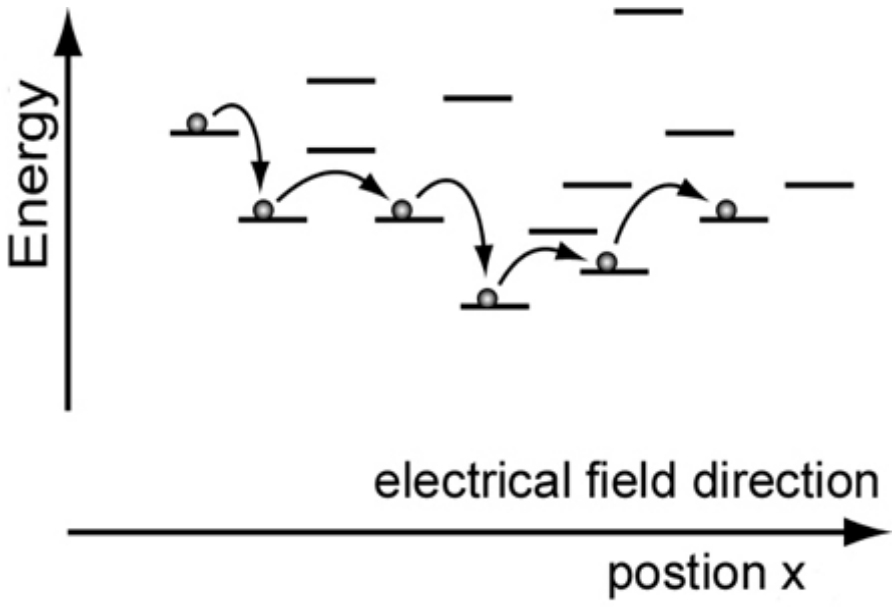


**Figure 1.10: the hopping charge transport mechanism in organic semiconductors.**

## 1.4 Exciton Formation and Dissipation

After the injection from the electrodes and the transport in organic materials, the charge carriers, electrons and holes, in OLEDs will recombine to form excitons. An exciton is a bound state of an electron and hole in an insulator or semiconductor, bound through Coulomb interaction. It is a quasiparticle of a solid, which provides a means to transport energy without transporting net charge. A vivid picture of exciton formation is as follows: a photon enters a semiconductor, exciting an electron from the valence band into the conduction band. The missing electron in the valence band leaves a hole behind, to which the electron is attracted by the Coulomb force. The exciton results from the binding of the electron with its hole. As a result, the exciton has slightly less energy than the unbound electron-hole pair.

Excitons can be classified into two cases (figure 1.11), depending on the strength of the electron-hole interaction. The strength of this interaction is determined by the screening effect of the surrounding lattice: polarized lattices, with high dielectric function, ε, screen the electron-hole attraction, resulting in a small exciton binding energy. At low temperatures, this results in a Wannier exciton, which has a spatial extent much larger than the lattice spacing of the molecule. In less polarized lattices (low ε), the high exciton

binding energy results in strongly bound Frenkel excitons, with a spatial extension of the same order as the intermolecular distance.

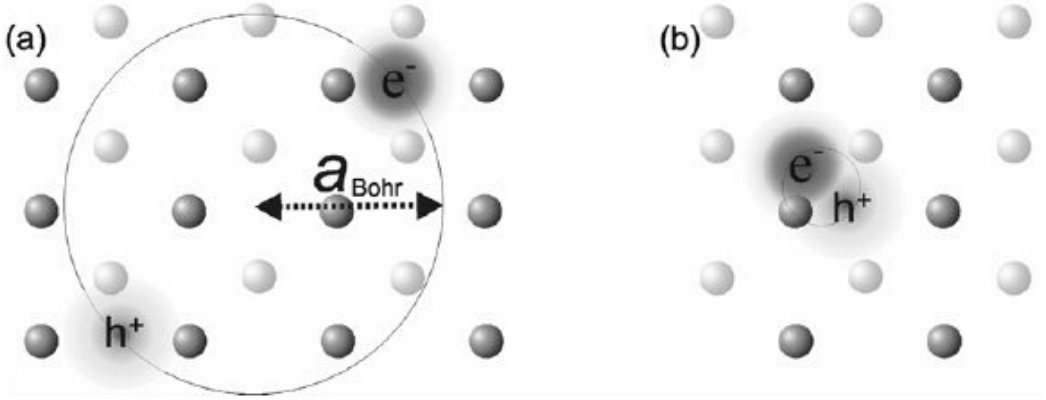


**Figure 1.11: Left: a pair of weekly bounded negative and positive carriers sitting on different molecules far apart (Wannier exciton). Right: an excited state sitting on one molecule (Frenkel exciton).**

The excitons contain two unpaired electrons in different orbitals, and they can be of the same spin or of different spin. Such states are triplet and singlet excited states respectively, and the two are distinct species with different physical and chemical properties. A triplet excited state has a lower energy than the corresponding singlet excited state because of the repulsive nature of the spin-spin interaction between electrons of the same spin. From a quantum mechanical view, singlet and triplet can be expressed as:

$$\left.\begin{aligned} |1,1\rangle &= \uparrow\uparrow \\ |1,0\rangle &= (\uparrow\downarrow + \downarrow\uparrow)/\sqrt{2} \\ |1,-1\rangle &= \downarrow\downarrow \end{aligned}\right\} \quad s = 1 \quad \text{(triplet)}$$

$$\left.|0,0\rangle = (\uparrow\downarrow - \downarrow\uparrow)/\sqrt{2}\right\} \quad s = 0 \quad \text{(singlet)}$$

The equations above theoretically predict that 25% of the excitons that are created from uncorrelated electrons and holes in operating OLEDs are singlet while 75% are triplet.

The excited states initially produced through the absorption of a photon are almost singlet excited states because practically all the organic molecules have a singlet ground state and the selection rules for absorption strongly favor the conservation of spin during the absorption process. The singlet-triplet

absorption can be observed with sensitive spectrometers, and it can be enhanced by the presence of a paramagnetic species such as molecular oxygen and heavy atom, however, such absorption is very weak in general.

Generally speaking, both singlet and triplet excited state are not long-lived (~ns for singlet excited state and ~ms for triplet excited state) in that they are forced to lose their energy within a period of time induced by quantum turbulence, collapsing to their ground state radiatively or non-radiatively. The processes responsible for the dissipation of the excited states are shown in the Jablonski-diagram in figure 1.12 [15] in which $S_0$ is the ground state, $S_1$ is the first singlet excited state, $S_2$ is the second singlet excited state, $T_1$ is the first triplet excited state, A is absorption of photons, F is fluorescence, P is phosphorescence, ISC is intersystem crossing and IC is internal conversion, respectively.

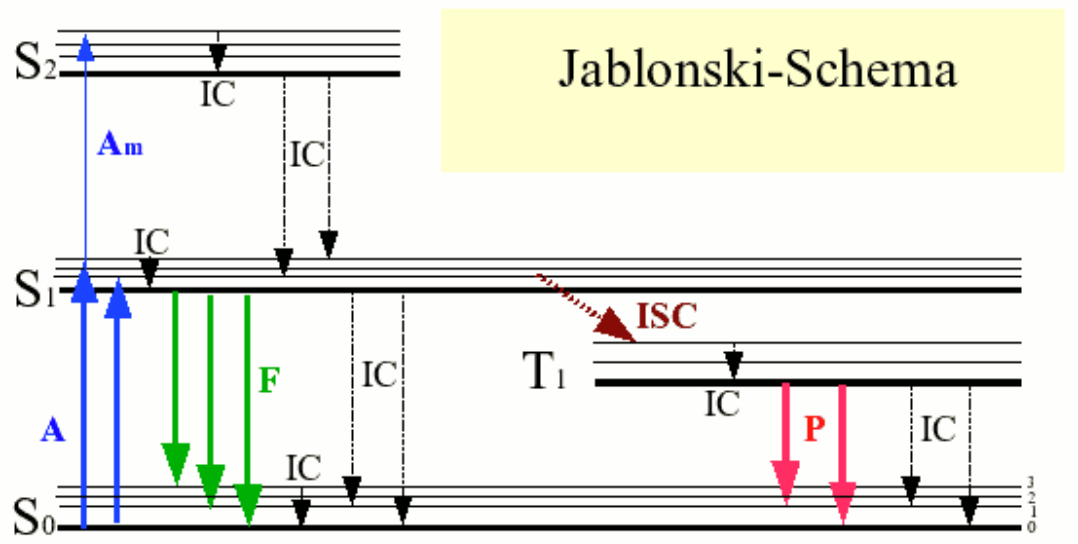


**Figure 1.12: Jablonski diagram showing some of the radiative and non-radiative processes available to molecules.**

It should be pointed out that those processes shown in Jablonski-diagram are competitive with each other in order to deactivate an excited state, and the relative magnitude of the rate constants determines the contribution given by each pathway.

Once a species is pumped up to an excited state from the ground state ($S_0 \rightarrow S_1$ or $S_0 \rightarrow S_2$), either through optical excitation or electron-hole pair recombination, the pathways for the dissipation of

electronic energy of the excited molecule can be classified into two major categories, radiative transitions and non-radiative transitions.

In radiative transitions, represented by solid lines in Jablonski-diagram, an excited species goes from a higher excited state to a lower one with the emission of a photon. There are three distinguishable processes in this radiative category:

(1) Fluorescence, which is colored in green, results from a rapid radiative transition (~ns) between states of the same multiplicity. The transition is mainly contributed by from $S_1 \rightarrow S_0$ transition although $S_2 \rightarrow S_0$ transition is occasionally observed and often hidden under the much more intense $S_1 \rightarrow S_0$ transition. Very weak $S_n \rightarrow S_m$ and $T_n \rightarrow T_m$ (n>m) fluorescence might be observed since they are spin allowed.

(2) Phosphorescence, which is colored in pink, is the result of a transition between states of different multiplicity, typically $T_1 \rightarrow S_0$; $T_n \rightarrow S_0$ is very rare. The rate constant of phosphorescence is usually much smaller than that of fluorescence in that phosphorescence is spin forbidden. However, the rate constant of phosphorescence can be dramatically increased by adding heavy atoms into the materials, which enables fast triplet dissipation due to strong spin-orbital coupling. Such molecular engineering is widely used in phosphorescent OLEDs.

(3) Delayed fluorescence, which is not shown in the Jablonski-diagram, differs from fluorescence because the measured rate of decay of emission is less than that expected from the $S_1 \rightarrow S_0$ transition. It results from either a process named triplet-triplet annihilation or the recombination of trapped charges. More detail on delayed fluorescence will be introduced in chapter 3.

On the other hand, non-radiative transitions, represented by dotted lines in Jablonski-diagram, occur between isoenergetic (degenerate) vibrational-rotational levels of different electronic states. Since there is no change in the total energy, no photon is emitted. There are two processes in this non-radiative category:

(1) Internal conversion is non-radiative transition between isoenergetic states of the same multiplicity. Such transitions between upper excited states such as $S_n \rightarrow S_m$ and $T_n \rightarrow T_m$ is are extremely rapid,

being responsible for the negligible emission from upper state. However, internal conversion from $S_1$ to $S_0$ is much slower that fluorescence could compete with it.

(2) Intersystem crossing, which is colored in brown, is a non-radiative transition between states of different multiplicity. The non-radiative deactivation from $T_1$ to $S_0$ is a process in competition with regular phosphorescence. The intersystem crossing from $S_1$ to $T_1$ is the fundamental principle used in phosphorescent OLEDs in which a tremendous amount of triplets are harvested. The non-radiative transition between $T_1$ and $S_1$ requires thermal activation of $T_1$ to a vibrational level isoenergetic with $S_1$.

## 1.5 Anthracene-based OLEDs and Degradation Mechanisms

OLEDs have attracted significant attention because of their unique advantages for flat panel display applications [16,17].However, the relatively limited EL stability especially of blue emitting OLEDs, which alongside red and green emitting OLEDs are needed full color OLED displays, continues to limit their commercialization [18,19]. In blue OLEDs, EL efficiency decreases rapidly during operation, usually limiting a device useful life (lifetime) to only a few hundred hours. In most cases, the decrease in brightness is also accompanied by a loss in blue color purity, thus also causing a shift in display color balance [20,21,22]. Several classes of blue emitter materials have been studied for OLED applications, and new materials have been developed [23,24,25,26,27,28].

Several classes of blue fluorescent materials have been synthesized and studied for OLEDs. Among those candidates, anthracene has been one of the earliest and most widely studied, owing to a number of attractive features [29], but its high susceptibility to crystallization is a major limitation. To circumvent this limitation, anthracene derivatives with bulky substituent side groups are developed [23] and 9, 10-bis (2-naphthyl)-2-t-butylanthracene (TBADN) shown in figure 1.13 emerges as one of the most promising ones, in terms of the color purity, quantum yield and EL stability [24]. However, the lifetime of TBADN-based OLEDs is still not long enough in comparison to its red and green counterparts and the degradation mechanisms of TBADN in both color purity and EL efficiency are still not well understood.

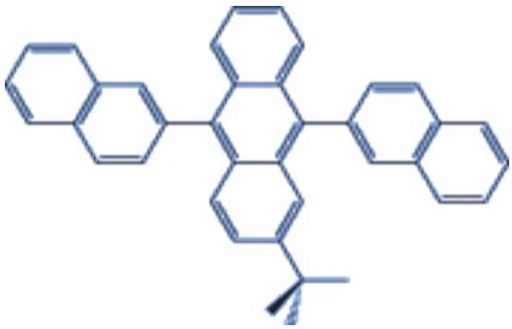

**Figure 1.13: Molecular structure of TBADN.**

In previous studies on the EL efficiency loss of TBADN-based OLEDs during electrical aging, three main degradation mechanisms are proposed, the breakdown of both organic/electrodes and organic/organic interfaces [22], narrow charge carrier recombination zone that results in concentrated molecular degradation [21] and the accumulation of aging-induced fixed positive charges that act as exciton quenchers[30,31].

However, these proposed explanations have some limitations, and cannot explain some experimental observations. For example, the change in I-V characterisitic after electrical aging does not necessarily indicate the breakdown of interfaces, and the correlation between device lifetime and the width of recombination zone does not provide further information on intrinsic device degradation, and the chemical nature of the accumulated charges is still unclear. In this thesis, the issue of the EL efficiency loss in blue OLEDs will be investigated through a molecular or intermolecular level, providing a new dimension to understand the EL degradation mechanism.

Besides the EL efficiency loss, another important issue which is somehow overlooked in anthracene-based OLEDs is the color purity loss during electrical aging, resulting in the color change from deep blue to greenish blue. So far no comprehensive study has been done to uncover the color purity loss, but only a few intuitive explanations were proposed such as the penetration of holes to ETL resulting in the recombination and emission from $AlQ_3$ [21,22]. In this thesis, compelling experimental evidences are obtained in order to fully understand the problem, which shed the light on an approach that could improve the color stability of blue OLEDs.

## 1.6 Objectives and Thesis Organization

In this thesis, the degradation mechanisms of anthracene-based OLEDs, including the molecular degradation in bulky organic fluorescent materials and the interfacial breakdown between organic/metal cathode interfaces, are mainly investigated by employing a number of techniques. This thesis is organized into six chapters, in which the latest and detailed experimental progress has been covered.

Chapter one is the introduction to OLEDs, including the historical background of organic electronics, the fundamental operating mechanisms and physics of OLEDs and the remaining obstacles in scientific research.

Chapter two is mainly related to the experimental aspect of OLEDs including substrate preparation, device fabrication and device testing.

Chapter three to chapter five, as the main body of this thesis, are discussing the polaron-exciton interactions, formation of the intermolecular species and the photo-degradation of organic / metal cathode interface, respectively. These three chapters are independent from each other although the delayed EL measurement, which is the key experimental means in uncovering the formation of the intermolecular species in chapter four, is particularly introduced in advance in chapter three.

Chapter six is the summary and the future works.

# Chapter 2

# Experimental Methods

Experimental methods involve the fabrication and testing of OLEDs. In this chapter, the fabrication of OLEDs is first introduced from the substrate preparation to the material deposition. After that, a number of measurement equipment and techniques that widely used in the investigation of the characteristics of OLEDs are introduced.

## 2.1 Fabrication of OLEDs

Device fabrication includes the indium tin oxide (ITO) substrate patterning, the substrate treatment and the thermal evaporation of the organic and metal materials. Each of these steps substantially determines the quality and performance of the operating OLEDs, which are the prerequisites for the device testing in the next section.

### 2.1.1 ITO Substrate Patterning

The glass substrates are initially coated with full ITO layer. Patterning the ITO substrate by using photolithography is to obtain ten independent ITO columns as the anode and four as the cathode contact pads. There are seven main steps involved in the ITO substrate patterning process.

**I. Substrate Preparation**

ITO substrates are put into a 1L beaker filled with 500mL water and 10mL micro-90 optical cleaner and are cleaned with ultrasound for 10 minutes to remove the inorganic particles on the surface of ITO. Then the ITO substrates are taken away from solution and gently agitated with Q-tips for about 1 minute for further cleaning the ITO surface.

After that, the ITO substrates are cleaned in Acetone and Isoproponal, two typical organic solvents that are widely used in cleaning, with ultrasound for 15 minutes, respectively, to remove the organic contaminations on the ITO substrates. Then a nitrogen gun is used to blow and dry the ITO substrates

before they are put into an oven at 125$^{o}$C for 30 minutes for further drying, which is good for promoting the adhesion between the ITO surface and the photoresist applied in next step by reducing the moisture content of the surface.

**II. Applying Positive Photoresist**

After cleaning the ITO substrates, the AZ 15-18 photoresist is coated on the ITO surface by using the spn-coating machine with the following set parameters: 3000 rpm, 50 s and 25 acceleration, which enable the formation of a thin, uniform film on top of ITO.

However, quick examination on the photoresist layer for visible defects such as dirt, photoresist voids and flares or uneven photoresist coverage is necessary. Once the coated photoresist layer is not perfect, the substrate should be placed into striper solution for 5 min to remove the photoresist layer and the substrate preparation procedure is repeated.

If the substrates with photoresist layer do not require reworking, they should be placed in a light-proof box in order not to be exposed to ambient light.

**III. Bake Photoresist: Soft Bake**

The ITO substrates are then put into an oven, which is preheated to 90$^{o}$C, for 30 min before they are removed from the oven. They are allowed to cool for 2 minutes.

**IV. Exposure**

Following the soft bake step, the substrates, now coated with photoresist, are attached with the metal mask by scotch tape and exposed to 405 nm UV from MA6 Mask Aligner for exactly 15 s. Since the table of MA6 Mask Aligner is transparent, a piece of black paper is recommended to be put on the center of the aligner table to reduce the reflection of UV light which might causes over exposure.

Once the exposure to UV is done, the substrates with photoresist are allowed to be exposed to ambient light.

**V. Development**

After exposure, the photoresist on the substrate that get exposed will be dissolvable in solvent for development while the rest of the area will not. Thus, the basket with substrates are put in the beaker filled with MF-314 (alkaline) developer kept at a temperature of 20-25$^{o}$C, ensuring that the entire surface of the ITO is immersed, for exactly 45 s. Then the substrates are removed from the beaker, and are washed with distilled water and dried with a nitrogen gun.

**VI. Hard Bake**

The ITO substrates are put into the oven, which is preheated to 120$^{o}$C, for 30 min before they are removed from the oven. They are allowed to cool for 2 minutes.

**VII. Etching**

In this step, the purpose is to remove the ITO that is uncovered by photoresist by immersing the substrates into acid solution. Once the temperature of the acid solution mixed from pour 200mL of water, 200mL of HCL (38%) and 20mL of $HNO_3$ (70%) reaches 56$^{o}$C on a hot plate, the basket with substrates is immersed into the acid solution for exactly 1 min to ensure complete etching.

After that, the basket is removed from the acid solution and immediately immersed into the distilled water to wash off the residual acid. After 2 or 3 minutes, a nitrogen gun is applied to dry the substrates and an ohmmeter is used to check the etched areas to see if they are non-conductive. If the etched areas are conductive, the substrate requires more etching. It could be done through the etching of another 15 s at the same temperature.

Once the etched areas, especially the edges of the substrate, become non-conductive, the substrates are put back into basket and immersed in striper solution for 5 minutes, continuously twisting the basket to ensure sufficient removing of photoresist.

Then the basket containing the substrates is removed from the striper solution and rinsed with DI water before the substrates are cleaned with Acetone and Isopropanol in ultrasound for 15 min, respectively.

Finally, the ITO substrates are put into an oven, which is preheated to 120$^{o}$C, for 30 min before they are removed from the oven.

The ITO substrate after patterning is shown in figure 2.1. The ten narrow columns are the ITO anode, and the four wider ones at the corners are the cathode contact pads.

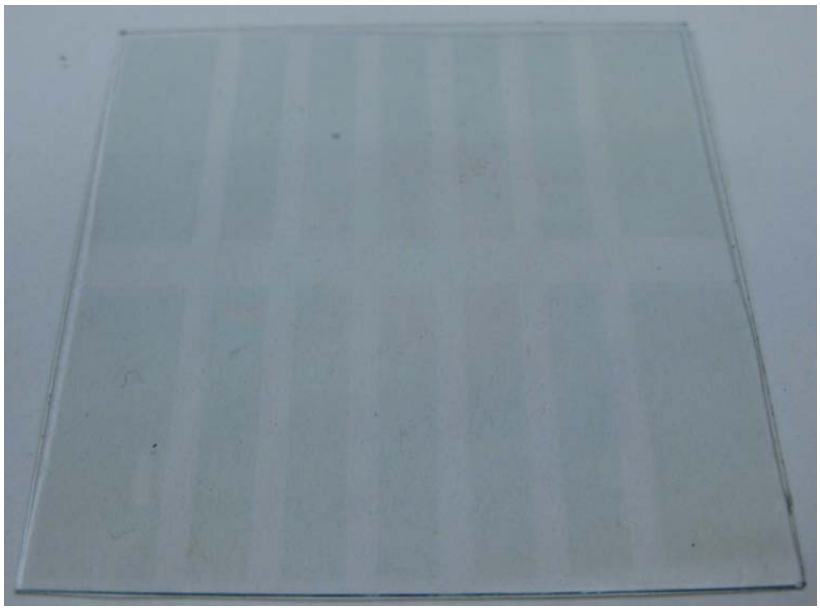

**Figure 2.1: ITO substrate after patterning.**

### 2.1.2 Applying Dielectric Layer

Practically, OLEDs with good quality and performance can be achieved on the patterned ITO substrate shown in figure 2.1. However, for certain special purposes, devices are preferred to be deposited on ITO with smaller area in which the edges of the ITO columns are not incorporated. For example, the photo-degradation study in chapter 5 requires the removal and re-deposition of the cathode [32], which cannot be fulfilled on a regular patterned ITO substrate due to the short pass at the ITO edge once the cathode is removed. Thus, ITO substrate with dielectric layer is needed.

Here, the dielectric layer is an insulator applied on the edge of ITO area, providing protection for the potential short pass of devices.

### VIII. Substrate Preparation

ITO substrates are put into a 1L beaker filled with 500mL water and 10mL micro-90 optical cleaner and are cleaned with ultrasound for 10 minutes to remove the inorganic particles on the surface of ITO. Then the ITO substrates are taken away from solution and gently agitated with Q-tips for about 1 minute for further cleaning the ITO surface.

After that, ITO substrates are cleaned in Acetone and Isoproponal, two typical organic solvents that are widely used in cleaning, with ultrasound for 15 minutes, respectively, to remove the organic contaminations on the ITO substrates. Then a nitrogen gun is used to blow and dry the ITO substrates before they are put into an oven at 125$^{o}$C for 30 minutes for further drying, which is good for promoting the adhesion between the ITO surface and the photoresist applied in next step by reducing the moisture content of the surface.

**IX. Applying Negative Photoresist**

After cleaning the ITO substrates, the SU-8 25 photoresist is coated on the ITO surface by using the spin-coating machine with the following set parameters: 6000 rpm, 50 s and 25 acceleration, which enable the formation of a thin, uniform film on top of ITO.

However, quick examination on the photoresist layer for visible defects such as dirt, photoresist voids and flares or uneven photoresist coverage is necessary. Once the coated photoresist layer is not perfect, the substrate should be placed into striper solution for 5 min to remove the photoresist layer and the substrate preparation procedure is repeated.

If the substrates with photoresist layer do not require reworking, they should be placed in light-proof box in order not to be exposed to ambient light.

**X. Bake Photoresist: Soft Bake**

The ITO substrates are put into an oven, which is preheated to 90$^{o}$C, for 30 min before they are removed from the oven. They are allowed to cool for 2 minutes.

**XI. Exposure**

After soft bake, the substrates coated with photoresist are attached with the negative mask by a scotch tape and exposed to 405 nm UV from MA6 Mask Aligner for exactly 15 s. Since the table of MA6 Mask Aligner is transparent, a piece of black paper is recommended to be put on the center of the aligner table to reduce the reflection of UV light which might causes over exposure.

Once the exposure to UV is done, the substrates with photoresist are allowed to be exposed to ambient light.

**XII. Bake**

The ITO substrates are put into an oven, which is preheated to 90$^{o}$C, for 30 min before they are removed from the oven. They are allowed to cool for 2 minutes.

**XIII. Development**

After exposure, the photoresist on the substrate that did not get exposed will be soluble in the developer while the rest of the area will not. Thus, the basket with substrates is put in the beaker filled with Propylene-Glycol-Methyl-Ether-Acetate (PGMEA) developer kept at a temperature of 20-25$^{o}$C, ensuring that the entire surface of the ITO is immersed, for exactly 6 min. Then the basket with substrates is removed from the beaker, and washed with Isoproponal and distilled water, respectively, and dried with a nitrogen gun.

If the negative mask has not been aligned properly, the substrates should be immersed into a beaker covered with an aluminum foil and filled with N-methylpyrolidine (NMP) photoresist remover which has been boiled for 30 to 45 min on a hot plate at 60 to 70$^{o}$C in order to remove the negative photoresist. Then the procedure needs to be started from substrate preparation.

**XIV. Hard Bake**

The ITO substrates are put into the oven, which is preheated to 120$^{o}$C, for 30 min before they are removed from the oven. They are allowed to cool for 2 minutes.

After the complete procedures described above, the substrate with dielectric layer is ready, which is shown in figure 2.2.

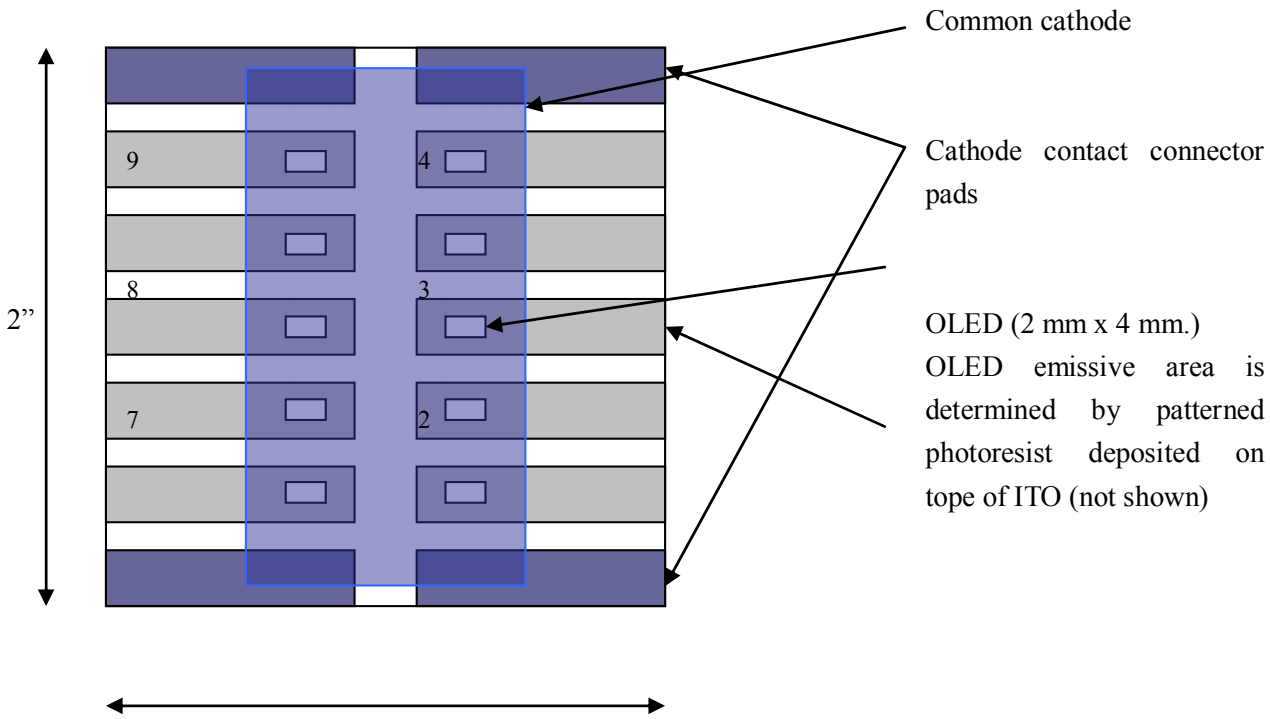


**Figure 2.2: Patterned ITO substrate with dielectric layer.**

### 2.1.3 Plasma Treatment

After step I to XIV, ITO substrates with dielectric layer are prepared. Before the device fabrication, further cleaning of the ITO substrate by using reactive ion etching (RIE) technology is necessary. RIE applies the plasma treatment to the ITO surface in order to improve the work function of ITO, and greatly improve the charge balance and device lifetime.

The optimal parameters of RIE for substrate treatment are:

Pressure: 20

Power: 100

Duration: 2min

Chemical Proportion: $CF_4$(75%):$O_2$(25%)

### 2.1.4 Deposition Parameters

In all the devices, ITO and Mg:Ag are used as hole-injecting anode and electron-injecting cathode , respectively. N,N′-di(naphthalene-1-yl)-N,N′-diphenyl-benzidine) (NPB) is used as a hole transport layer (HTL). Tris(8-hydroxyquinoline) aluminum ($AlQ_3$), bis(2-methyl-8-quinolinate)4-phenylphenolate (BAlQ) and 4,7-diphenyl-1,10-phenanthroline (BPhen) are used as electron transport layers (ETL). TBADN and ADN are used as emitting layers (EML). Specific device structures are described in the corresponding chapters of this thesis. All devices are fabricated by deposition of the organic materials and the cathode metals at a rate of 0.3-3 Å/s using thermal evaporation at vacuum base pressure of about 5 x $10^{-6}$ torr on UV ozone-cleaned ITO-coated glass substrates.

## 2.2 Testing of OLEDs

After the device fabrication, all the testing and measurements of OLEDs are carried out in nitrogen atmosphere which prevents the ambient degradation. Some fundamental features of OLEDs could be quickly obtained such as driving voltage, brightness and I-V-L characteristics through certain basic measurements. However, some other device testing involves a number of complicated experimental measurements in much longer time scale such as the EL stability measurement, the delayed EL measurement and the photodegradation measurement.

### 2.2.1 EL Stability Measurement

For EL stability measurement, the devices are driven by alternating current with a 50%duty cycle and a frequency of 100Hz so that the effect of charge accumulation on device EL can be ruled out. A photodiode is used to collect the EL signal. Both of the EL intensity and driving voltage as functions of time are recorded by a computer during device aging. The experimental setup is shown in figure 2.3.

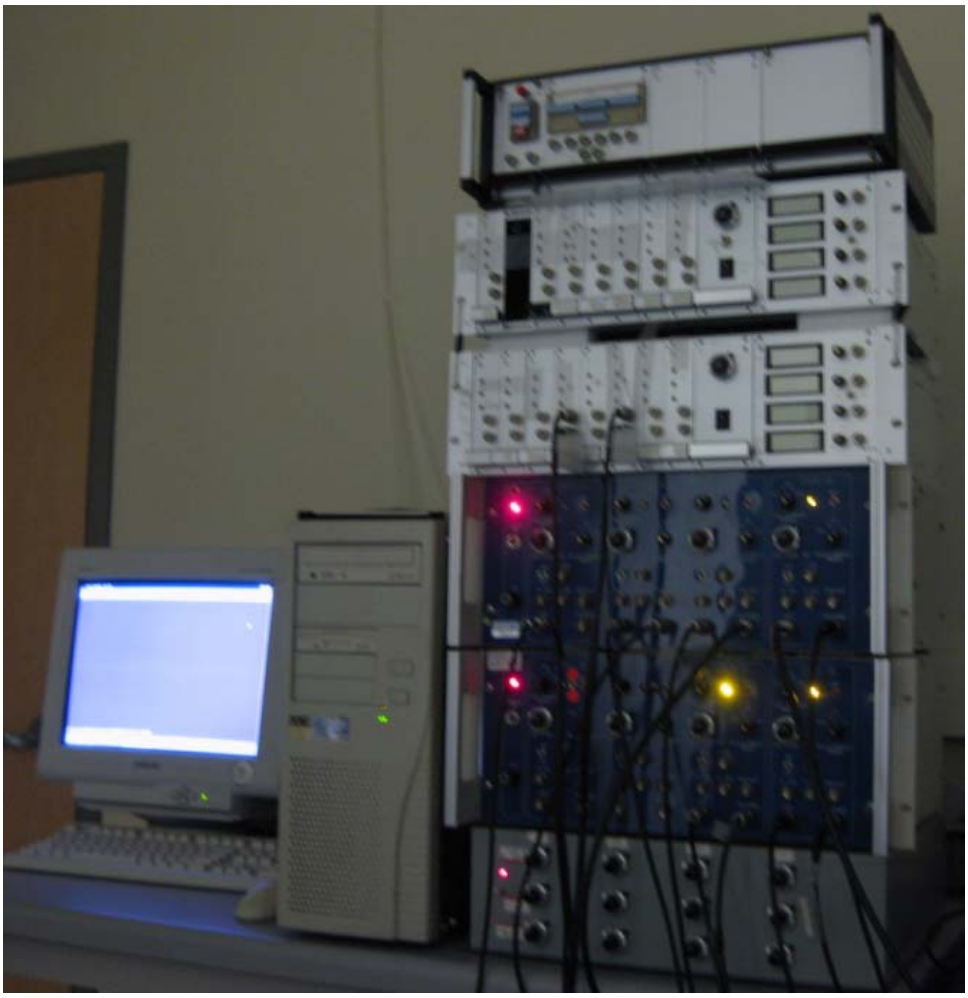

**Figure 2.3: Experimental setup for EL stability measurement.**

### 2.2.2 Delayed Electroluminescence Measurement

For delayed EL measurement, the experimental setup is schematically shown in Figure 2.4 [33]. Emitting light of OLEDs is connected to a photodetector through a fiber-optic bundle with a light chopper sitting in between [Figure 2.4(a)]. The timing of forward and reverse bias is shown in Figure 2.4(b). During the application of forward bias, the chopper blade prevents light from reaching the photodetector (this is important in order to prevent photodetector saturation) and the devices are driven using a square pulse driving scheme, with a forward bias of 10 V and a pulse width of 0.5ms (i.e. sufficiently long to ensure prompt EL reaches its steady-state intensity). When the forward bias is turned off, light reaches the photodetector. After a certain time delay, typically of about 0.5 ms which is significantly longer than

fluorescent singlet lifetime (~ 20 ns) to ensure the absence of any contributions from prompt EL in the collected signal, a 0.5ms reverse bias pulse is applied to the sample to test the effect of reverse bias on delayed EL intensity and the time evolution of delayed EL signals are collected.

For detection of time-resolved emission an R928 photomultiplier tube equipped with a 700-nm short-wavelength pass filter, which was necessary to eliminate the spurious signal originating from the light chopper (IR LED—photodiode combination used to derive chopper timing signals), is used. The photomultiplier current was amplified by an Ithaco Model 1211 current preamplifier and the time evolution of delayed light emission was recorded by a Tektronix digital oscilloscope. Typically, the measurement was averaged for about 10 000 sweeps. Variable OLED forward and reverse biases were supplied by a homebuilt operational amplifier driven by a Stanford Research Systems Model DG535 Digital Delay Generator. The wavelength dependence of delayed EL was determined using an Ocean Optics Model S2000-FL fiberoptic spectrometer equipped with a linear charge-coupled device (CCD) array. The whole experiment was controlled by a personal computer using suitable data acquisition cards and general purpose interface bus (GPIB) interfaces. The experimental setup is shown in figure 2.5.

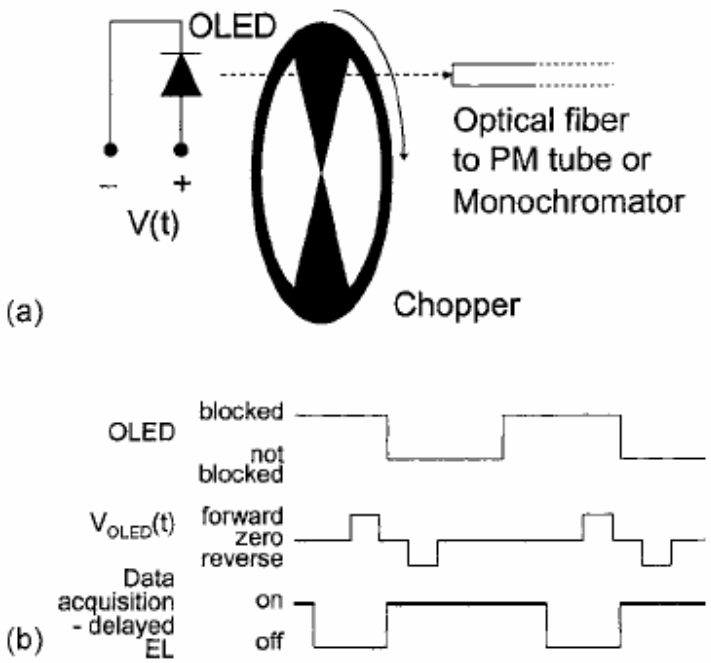


**Figure 2.4: Schematic diagram of delayed EL experiment.**

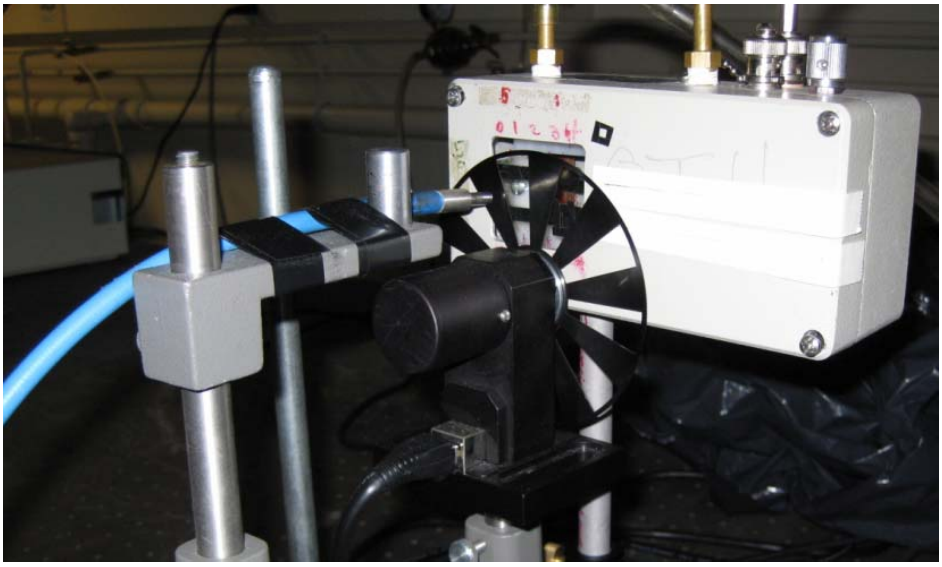

**Figure 2.5: Experimental setup for delayed EL measurement.**

### 2.2.3 Photo-stability Measurement

For irradiation test, the experimental setup is schematically shown in Figure 2.6. OLEDs are exposed to monochrome illumination at different wavelengths from a 200W Hg-Xe lamp equipped with Oriel-77200 monochromator. The power intensity of the irradiation spot is varying at different wavelength, roughly from 0.5mW/cm$^2$ to 2mW/cm$^2$. Simultaneously external voltage is applied in order to obtain the current density of 0.5mA/cm$^2$ flowing through the device. During the stress condition of irradiation and current flow, the time-resolved EL and driving voltage of devices are measured by spectrometer and voltmeter, respectively. The experimental setup is shown in figure 2.7.

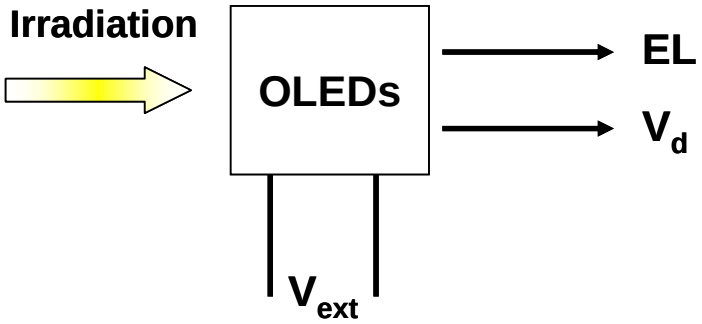


**Figure 2.6: Schematic diagram of irradiation test.**

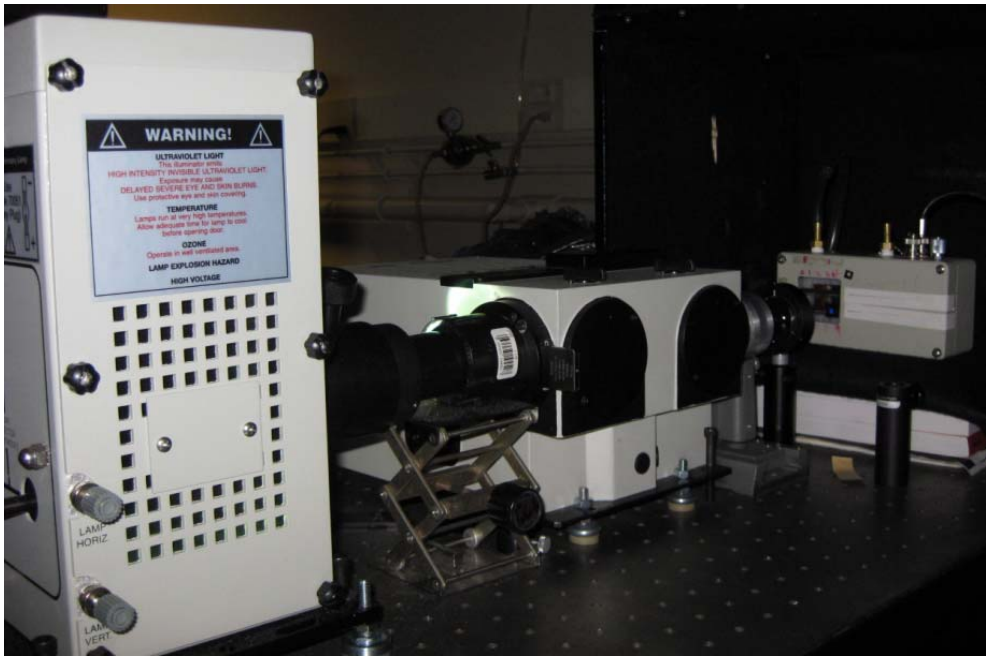


**Figure 2.7: Experimental setup for photo-stability measurement.**

# Chapter 3

# Delayed EL and Polaron-Exciton Interactions

Quantum mechanically, the recombination of electrons and holes in OLEDs produces both singlet and triplet excited states in the ratio of 1:3 approximately. In fluorescent OLEDs (as in case of the OLEDs studied in this thesis), the singlet excited states dissipate very quickly (~ns) while the triplet excited states last much longer (~ms). Since the triplets are longer lived (which indicates longer diffusion length), they have a much higher possibility to interact with each other. As a result, the delayed EL is the main dissipative way accounting for the intermolecular interaction among those long-lived triplets, and the detection and analysis of the delayed EL signal provides important information on the exciton dynamics and polaron-exciton interactions within the device.

In this chapter, firstly the fundamental physics and characteristics of delayed EL are introduced. Then with the knowledge of delayed EL, the polaron-exciton interactions in various types of OLEDs are studied.

## 3.1 Delayed EL

Delayed EL is the observed emitting light after external bias is removed. It originates from two different processes: triplet-triplet annihilation (TTA) and recombination of trapped charges.

TTA is a bimolecular interaction in which an interaction between two triplets results in the production of one singlet excited state and one ground state. TTA can be described by the following two steps

(1) $T_1 + T_1 \rightarrow X \rightarrow S_1 + S_0$

(2) $S_1 \rightarrow S_0 + \text{photon}$

where $T_1$, $S_1$ and $S_0$ are first excited triplet state, first excited singlet state and ground singlet state, respectively. In this scheme, equation (1) represents a TTA process including the bimolecular

recombination of two triplets, the formation of certain intermediate entity X and the production of excited and ground singlet states, and equation (2) represents the radiative relaxation of the singlet exciton produced in step (1), contributing to delayed EL.

The recombination of trapped charges is the process that trapped charge carriers are thermally released and combine to form singlet excitons. Delayed EL from the recombination of trapped charges is usually observed in host:guest systems in which charges are trapped on guest sites.

Those above two processes can be distinguished by studying their distinct behaviors towards applying and removing the reverse bias during delayed EL, as shown in figure 3.1 [33]. In figure 3.1(a), the decrease in delayed EL observed when applying the reverse bias is due to the electrical field-induced dissociation of singlet excited states formed from TTA. Such dissociation of singlet excited states lasts until the reverse bias is removed and the intensity of delayed EL recovers fully to the level with zero reverse bias. The reason that the triplet excited states are not dissociated into free charges by reverse bias is because triplets have higher binding energy than singlets. In figure 3.1(b), the substantial decrease in delayed EL observed when applying the reverse bias is due to the trapped charges being swept by the electrical field. When the reverse bias is removed, the delayed EL does not recover. It is worthwhile to mention that sometimes the delayed EL contains the contributions from both of the two processes, in which in a partial recovery is observed when the reverse bias is removed.

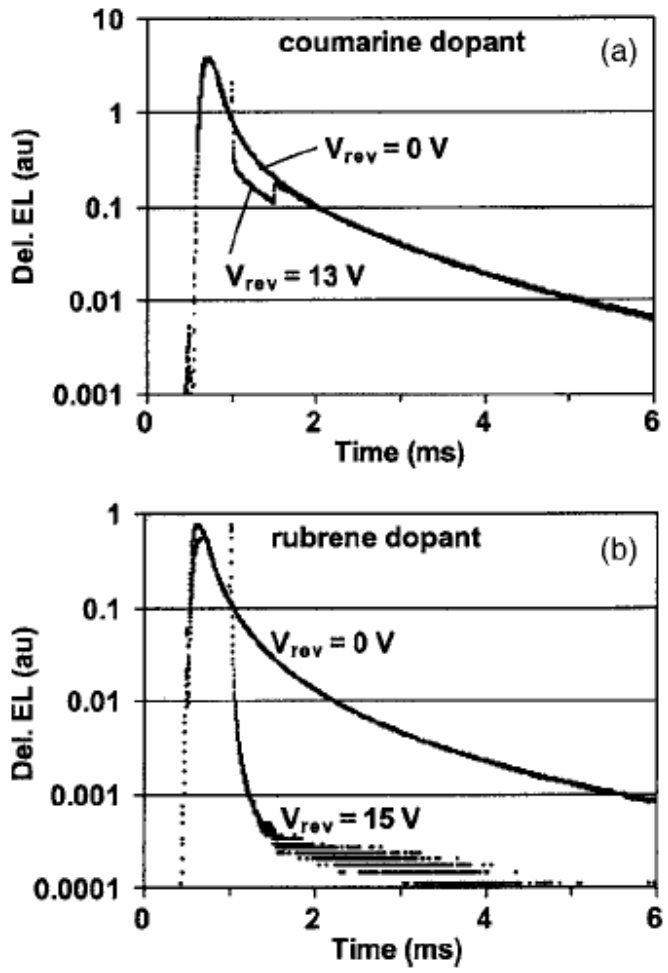


**Figure 3.1: Time evolution of delayed EL for two different reverse biases. (a) Coumarine dopant. (b) Rubrene dopant [33].**

## 3.2 Polaron-Exciton Interactions

A polaron is a quasiparticle composed of a charge and its accompanying polarization field. A slow moving electron in organic materials, interacting with lattice ions through long-range forces, will permanently be surrounded by a region of lattice polarization and deformation caused by the moving electron. The polaron-exciton interactions are extremely important in OLEDs because the quenching of excitons by the accumulated charges, as a result of polaron-exciton interaction, is greatly limiting the EL efficiency of OLEDs. The interaction between the polarons and the singlet excited states can be studied in a straightforward way in that the singlet excited states can be created through optical excitation directly.

Contrarily, the interaction between the polarons and the triplet excited states is not easy to be investigated due to the difficulty in observing the emission of non-radiative triplet excited states. Now with the knowledge of delayed EL resulting from the TTA, we can precisely monitor the change of triplet concentration as a function of time and thus study the polaron-exciton interaction.

In figure 3.2, NPB and TBADN are used as HTL and EML, respectively. The delayed EL intensities of devices with different ETLs such as $AlQ_3$, BPhen and the combination of these two are compared. As the figure shows, there are complete recoveries of delayed EL intensity when reverse bias is removed, indicating that the delayed EL is caused by the TTA. The driving voltage of device with BPhen as ETL is lower than that with $AlQ_3$ as ETL because BPhen has higher electron mobility and lower LUMO level than $AlQ_3$..

The trend of the decreasing delayed EL from $AlQ_3$ to BPhen ETL as a result of the forward bias with the same current density and time duration in the figure 3.2 is showing the effect of triplet quenching by polarons on delayed EL intensity. In the device with BPhen as ETL, triplets are greatly quenched by the highly injected electrons because of BPhens higher electron injection and transport ability than $AlQ_3$, thus resulting in lowest delayed EL intensity. In the other two cases, the device with $AlQ_3$ as ETL is giving the highest delayed EL intensity, and the device with the combination of the two ETLs is accounting for the medium delayed EL intensity. The result is clearly showing that the extensive injection of charges does not necessarily lead to higher concentration of triplet formation, but the over injection of charges or the accumulation can cause serious triplet quenching.

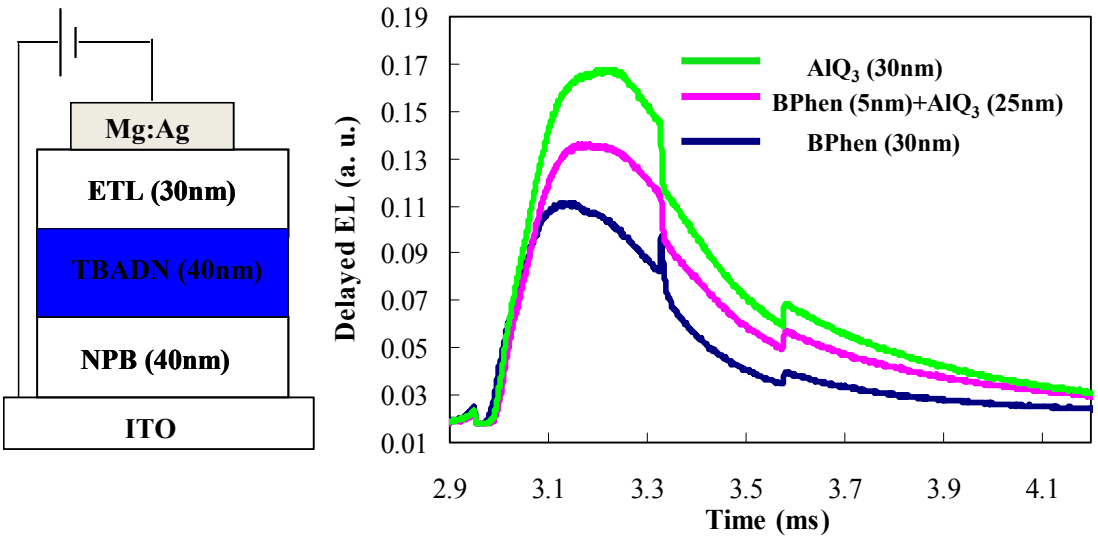


**Figure 3.2: Left: device structure with different ETLs. Right: Delayed EL intensity as a function of time from OLEDs with three different ETLs.**

Figure 3.3 is showing the delayed EL as a function of time in NPB/TBADN:CBP/BPhen devices with different concentrations of CBP. As is well known, the hole mobility of CBP is higher than its electron mobility and thus it plays as a electron-hindering material. When the concentration of CBP increases from 0% to 30%, the intensity of delayed EL increases and reaches the maximum, suggesting that the effect of triplet quenching by electrons is reduced and the charge balance in EML is improved. However, if the concentration of CBP further increases up to 70%, the intensity of delayed EL decreases dramatically to the level where 0% CBP case stands. In this scenario, the extremely high concentration of CBP in TBADN leads to the over injection of holes, and thus the triplets are greatly quenched due to the charge unbalance.

Interestingly, we also find that the lifetime of triplet excited states, calculated from the time during which the delayed EL intensity decreases to half of the initial value, increases as the concentration of molecular spacer CBP increases. For instance in figure 3.3, the 0% CBP device has a triplet lifetime of 0.2 ms while the 70% CBP deivce has a triplet lifetime of 2 ms. The gradual change of triplet lifetime as a function of CBP concentration is indicating that the TTA is a short range interaction [34,35].

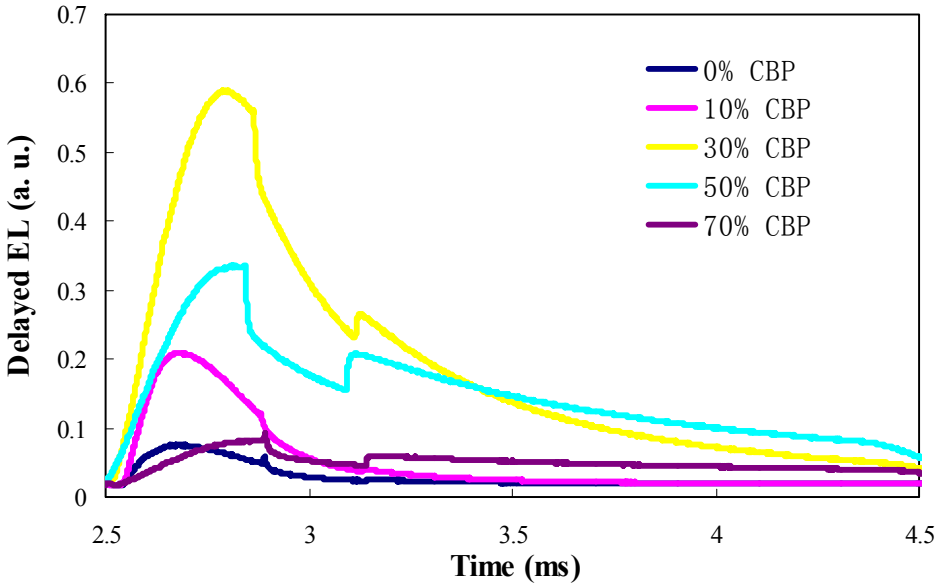


**Figure 3.3: Delayed EL intensity as a function of time in NPB/TBADN:CBP/BPhen devices with different concentrations of CBP.**

Besides polaron-triplet interactions, polaron-singlet interactions are also investigated in order to obtain a more complete picture of polaron-exciton interactions in OLEDs. Figure 3.4 and 3.5 show the hole- and electron-only current devices with blocking layers. Their PL spectra as a function of current density (with the excitation wavelength at 400nm and the optical power intensity 1.2 mW/cm$^2$) are shown inset. As the figures depict, when hole- and electron-only currents are applied, the PL efficiencies decrease almost 20% compared to the scenarios in which no currents are applied, suggesting the obvious quenching of the singlet excited states by the accumulation of charges. However, if the blocking layers are removed in both cases, the differences of the PL efficiencies between the cases when the current is applied and not disappear, which are shown in the insets of the figures. The results are indicating that the singlet excited states can be quenched by the accumulation of charges as well, although they are less sensitive to the quenching by charges than triplet excited states since singlets (~ns) have several orders of magnitude shorter lifetime than triplets (~ms).

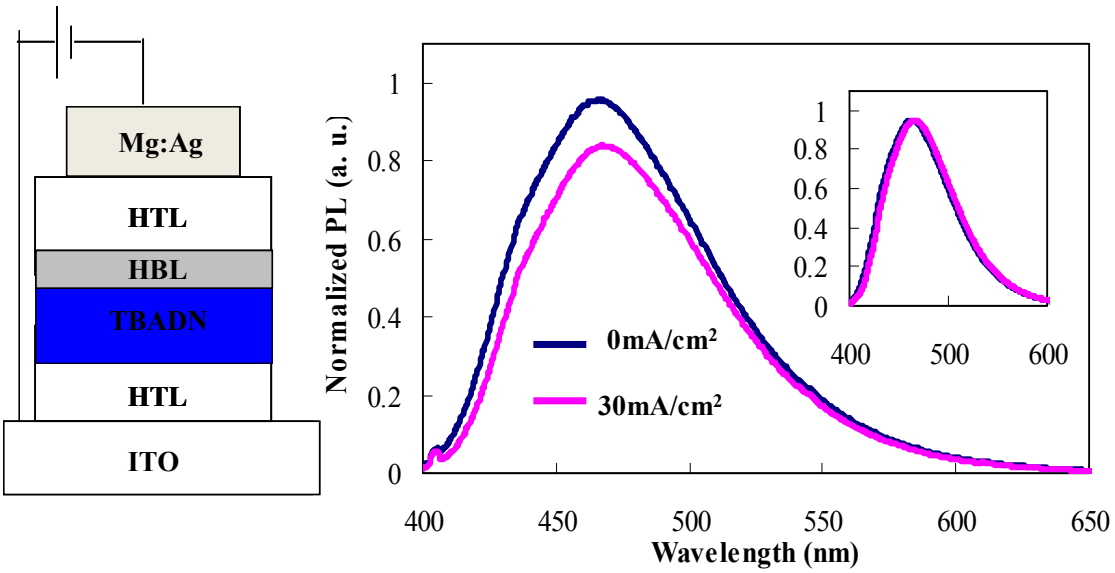


**Figure 3.4: Left: structure of hole-only current device. Right: Changes of PL spectral of device with and without (inset) hole blocking layer.**

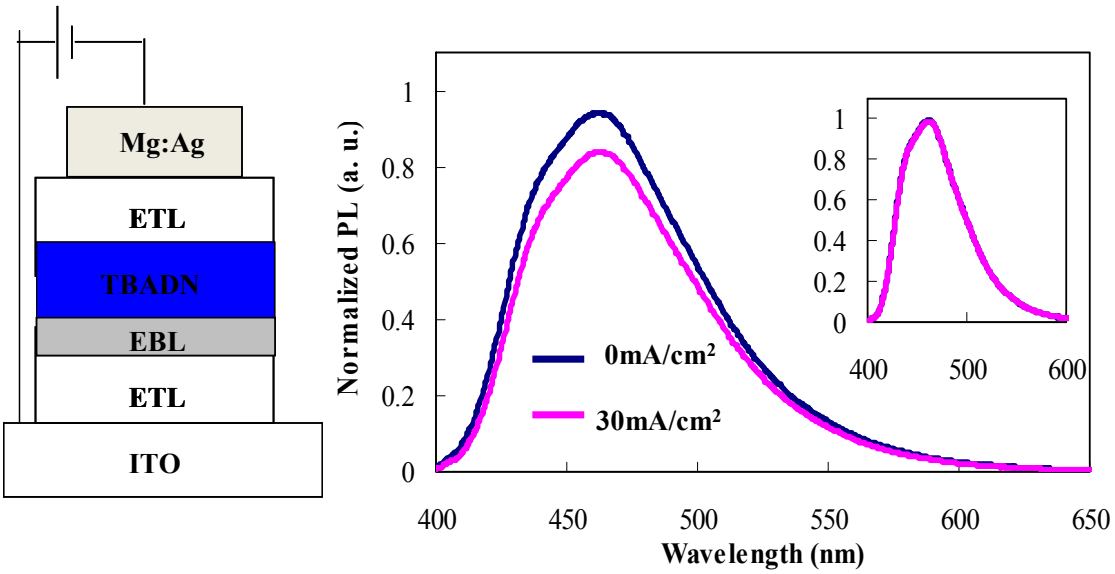


**Figure 3.5: Left: structure of electron-only current device. Right: Changes of PL spectral of device with and without (inset) electron blocking layer.**

However, it is reasonable to argue that the constancy of PL efficiencies as a function of current density in devices without blocking layers is because the density of optically created singlet excited states

is too low compared to the density of electrically created triplet excited states. Thus, the comparison of the effect of the quenching of singlets and triplets by polarons is further studied simultaneously. The device with the structure of ITO/NPB/TBADN/$AlQ_3$/Mg:Ag is aged at the current density of 20mA/$cm^2$ for 100 h until the prompt EL efficiency decreases 50% of the initial value. Then the delayed EL intensity is measured and it decreases 90% of the initial intensity (in figure 3.6). It means that a much larger amount of triplet excited states are quenched by the electrically-induced accumulated charges [34], given the fact that the concentration of triplet is comparable to that of singlet since both of them are created through charge injection and electron-hole pair recombination.

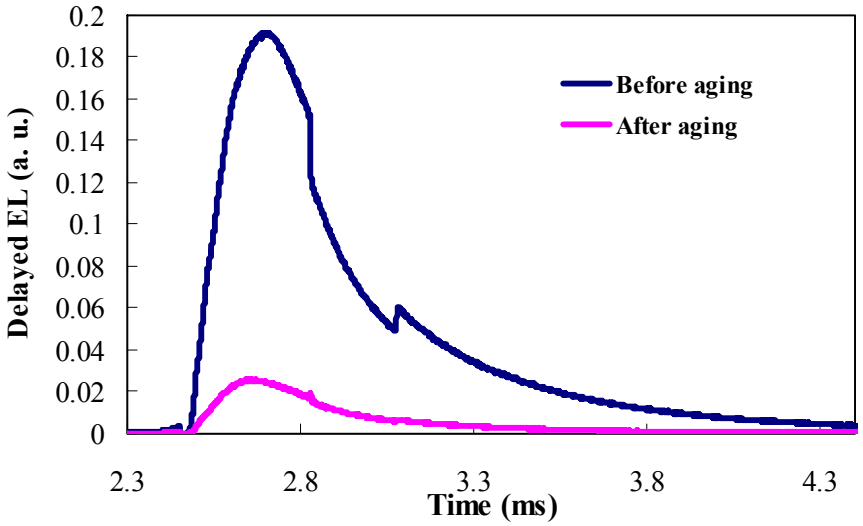


**Figure 3.6: Delayed EL intensity as a function of time before and after electrical aging.**

# Chapter 4

## Molecular Aggregation in Anthracene-based OLEDs*

A number of studies have addressed the EL stability of anthracene derivatives in general and of TBADN in particular. In their studies, Jarikov *et al* [36] ruled out the role of unipolar current on TBADN EL degradation, which is different from the case of green OLEDs based on $AlQ_3$ [18] and suggests fundamentally different degradation mechanisms. Kondakov *et al*. [30] demonstrated, using capacitance measurements, that the loss in luminance as a result of electrical aging in TBADN OLEDs was correlated with the accumulation of space charges in the light emitting layer of an OLED, suggesting that aging may be associated with charge trapping. However, the aging-induced trapped charge and its formation mechanism remain not well understood. In another report, Gong *et al*. [37] gave direct evidence of molecular aggregation in host-guest system due to Joule heating, providing important insights about the role of such aggregation in OLEDs degradation. Although such degradation mechanism can be expected to play a significant role in aggregation prone materials such as 9, 10-bis (2-naphthyl) anthracene (ADN), its role in materials with bulky and less symmetric molecular structures, such as in case of TBADN, has not been studied, and can be expected to be limited. In conclusion, the exact mechanisms behind EL aging in this important class of emitters remain unclear.

Figure 4.1(a) shows normalized EL spectra from a device of structure ITO/NPB/TBADN/$AlQ_3$/Mg:Ag, collected before and after electrical driving for 100 hrs at an average current density of 20mA/cm$^2$ using a standard AC driving scheme [38]. The spectra show a peak at 460nm characteristic of TBADN singlet emission (S1$\rightarrow$S0). The relative peak intensity of the spectrum collected after the electrical driving was about 40% lower (observed in the non-normalized spectra; not shown here), reflecting the expected decrease in EL efficiency (electrical aging) as a result of the prolonged electrical driving. As can be seen from the figure, the spectrum collected after the electrical

* The main content of this chapter was published in JAP [39], and was reproduced here by the permission from AIP.

stress period shows a significant peak broadening [39], signifying increased tail/peak emission ratio in the 500-575 nm range. (note: spectra of devices fabricated on the same substrate but left un-operated do not show any change over the same period of time, indicating that the peak broadening is primarily due to the electrical stress), The Commission Internationale de L'Eclairage (CIE) color coordinate are also measured at the beginning and the end of the electrical stress period and found to be (0.15, 0.12) and (0.19, 0.23), respectively, reflecting the consequent loss in color purity. To examine if the increased 500-575nm emission, and the corresponding loss in color purity, is due to emission from $AlQ_3$ ETL (which is a green luminescent material), perhaps due to a shift in recombination zone with electrical aging [40], we tested OLEDs in which BPhen is used instead of $AlQ_3$ as ETL. As can be seen from figure 4.1(b), EL spectra from the devices with the BPhen ETL show a very similar peak broadening in the 500-575 nm range after electrical aging, indicating that the effect is not due to $AlQ_3$ emission. In fact, mathematical calculation of the spectral shift (subtracting the initial spectrum from the final spectrum) reveals that the shift with electrical aging is almost identical in both devices (figure 4.1(c)), and corresponds to the emergence of a broad emission band in the 500-575nm range with a peak at around 535nm. The small difference in the spectra in figure 4.1(c) is possibly due to small variations in optical interference associated with small shifts in recombination with the different ETLs.

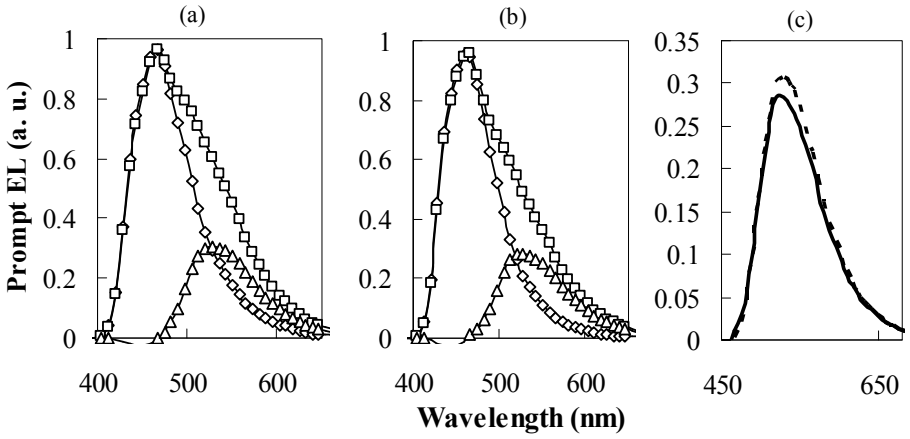


**Figure 4.1: Prompt EL spectra of OLEDs with (a) $AlQ_3$ and (b) BPhen as ETLs before and after aging.**

In order to gain more insights about this behavior, we used delayed EL measurements (measuring persistent EL in an OLED after the electrical bias is turned off) to study the same device. The technique allows distinguishing between the roles of triplet-triplet-annihilation (TTA) and recombination of de-trapped charges in producing the observed delayed emission and is effective in shedding the light on various bimolecular (exciton-exciton, polaron-exciton) interactions in OLEDs [41,42]. Figure 4.2 displays delayed EL spectra from the same devices, obtained before and after the same electrical stress period, and collected 0.2 ms after the forward bias pulse. As evident from the figure, all delayed EL spectra show a well resolved green emission band, with a peak around 535 nm, at the same wavelength corresponding to the elevated tail of the prompt EL spectra of the aged devices (Fig 4.1). As seen in figure 4.2, the total delayed EL intensity decreases rapidly with electrical aging, but the decrease in the green emission band occurs more slowly, leading to an apparent color shift. These results show that the loss of color purity of prompt EL with electrical aging in these devices is associated with a distinct emission band, with a peak at around 535 nm, whose intensity decreases at a rate slower than that of the main 460nm TBADN singlet emission band, resulting in a higher green/blue (535nm/460nm) emission ratio with electrical aging.

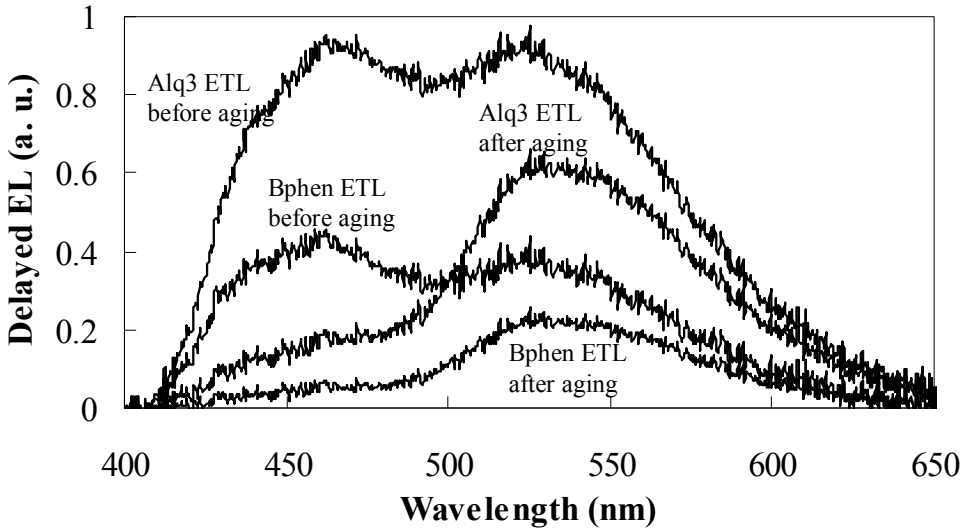


**Figure 4.2: Delayed EL spectra of OLEDs with $AlQ_3$ and BPhen as ETLs before and after aging.**

In general, the observation of a longer wavelength emission band with slower electronic transition kinetics in comparison to the 460 nm TBADN $S_1 \rightarrow S_0$ transition (the slower kinetics are evident in its higher relative intensity in delayed EL spectra compared to that in prompt EL spectra, which are collected ~0.2 ms after the forward bias is turned off) may, on a first sight, suggest that the 535 nm emission could be due to some triplet emission. However, triplet energy of anthracene chromophores is typically around ~1.8eV [43] (i.e. corresponds to 720 nm), and therefore does not correspond to the observed 535 nm emission peak. As singlet and triplet excited states of anthracene derivatives are generally located on the anthracene chromophores rather than on side groups [44], their singlet and triplet energies are generally expected to be very similar to those of anthracene. In addition, triplet to singlet transitions ($T_1 \rightarrow S_0$) in anthracene chromophores are disallowed on spin grounds, and are therefore generally very inefficient. This makes their easy detection at room temperature (or perceiving them by the unaided human eye in electrically-aged TBADN OLEDs in the form of color change) rather unexpected. Preliminary analysis therefore suggests that the 535nm emission is unlikely to be due to TBADN triplet emission.

In order to investigate the nature of the phenomenon behind the 535nm emission, we studied differences in the response behavior of the delayed EL characteristics to a reverse bias pulse before and after OLED electrical aging. Figure 4.3 shows the effect of applying a reverse bias pulse on delayed EL time decay characteristics in a device of structure ITO/NPB/TBADN/$AlQ_3$/Mg:Ag before and after electrical aging for 100 hrs at an average current density of 20mA/$cm^2$ . In this figure, the x-axis represents the time elapsed after the end of a 0.2 ms square forward bias pulse; where the forward bias pulse width is chosen to be sufficiently long to allow the prompt EL to reach its steady-state intensity. The delayed EL collection time scale (~ms) is much longer than typical singlet excited state lifetimes ( << 100 ns) [45], ensuring that the absence of any contributions from prompt EL in the collected signal. This delayed EL collection time scale delay is also at least 10x larger than typical OLED electrical time constant [46], rendering electrical transient effects negligible. As can be seen from the figure, in both cases (i.e. before and after device electrical aging), the application of a 0.25 ms reverse bias pulse (starting at 3.33 ms and ending at 3.58 ms on the figure, and of magnitude equal to 10 Volts) leads to a sudden decrease in OLED delayed EL intensity. The overall response behavior is however different in the

two cases. Before electrical aging, OLED delayed EL intensity recovers almost completely at the end of the reverse pulse, returning almost completely to its original decay trend. The almost complete recovery indicates that TTA is the dominant mechanism behind the observed delayed EL in this case [33,42]. After aging, on the other hand, the application of the reverse bias leads to a spike followed by a rapid decrease in delayed EL intensity, and its removal leads to only a modest (i.e. partial) recovery, leaving a mostly permanent (irreversible) decrease in delayed EL. Both the spike at the beginning of the reverse bias and the incomplete recovery at the end of the reverse bias indicate that delayed EL is primarily due to recombination of charge carriers in this case [33]. As some of these carriers will be swept away from the recombination zone towards the electrodes by the reverse bias field, the recovery of delayed EL at the end of the reverse bias pulse is incomplete. The delayed recombination of these carriers (i.e. their recombination after the forward bias is removed) indicates that they are initially trapped, hence are retarded from recombining until they become de-trapped (perhaps by thermal excitation). These results therefore reveal that the increasing 535nm/460nm emission ratio in delayed EL spectra with device aging is predominantly caused by delayed recombination of trapped charges. As the emission wavelength is different from that of TBADN singlet state, it follows that some other species, with a characteristic emission peak at 535 nm, is involved in this process. The longer emission wavelength indicates that this species may have a HOMO/LUMO energy gap significantly narrower than that of TBADN, hence can possibly act as a deep trap for electrons and/or holes, suggesting it may itself be playing a role in the charge trapping process. Light emission from this species can be due to energy transfer from the wider energy gap TBADN and/or, more likely in this case, due to its acting as an electron-hole (e-h) recombination center. It should be pointed out that the sudden decrease in delayed EL upon the application of the reverse bias pulse indicates that the 535 nm emission (which is the main component of delayed EL after device aging as shown in figure 4.2) is indeed not due to direct triplet emission ($T_1 \rightarrow S_0$) as was deduced above, since triplet excitons are generally not sensitive to electric fields. [Supplemental information: Triplet excitons are neutral, and also, unlike singlet excitons, are not appreciably susceptible to electric field dissociation, owing to their lower energy. Those two factors make them largely insensitive to electric field.].

It is also worthwhile pointing to the more significant decrease in the 460 nm emission intensity with electrical aging displayed by delayed EL measurements versus that displayed by prompt EL measurements (~90% and 40% reduction in 460 nm peak height in delayed EL and prompt EL, respectively, after driving for a period of about 100 hours), which is also consistent with previous reports [33]. Such difference in decay rates despite the fact that they both arise from the relaxation of TBADN singlet excitons ($S_1 \rightarrow S_0$) reveals that the singlet exciton populations in the two cases are produced through different paths, i.e. (i) produced via TTA process in case of delayed EL, and (ii) produced directly by e-h recombination in case of prompt EL. As triplet exciton lifetime is much longer than singlet exciton lifetime, they have much larger diffusion lengths, and therefore are more easily quenched by charges. As such, they become more efficiently quenched in aged devices due to the higher density of trapped charges, rapidly limiting the TTA process, hence resulting in the much faster decrease in the 460 nm emission peak in case of delayed EL. It should also be pointed out that the height of the spike observed at the beginning of the reverse bias is found to increase with OLED electrical stress time. The observations, therefore, fully support the conclusion that the increasing 535nm/460nm emission ratio observed with electrical aging is associated with recombination of trapped charges that increase in concentration with prolonged electrical driving of the OLEDs. Some species capable of weak green emission, with an emission peak around 535 nm, is involved in this recombination process, and possibly also in the charge trapping process. Contrarily, if other mechanisms, such as the breakdown of interfaces or the chemical reaction of molecules, are the main cause in luminance losses, then the prompt and delayed EL would be expected to decrease at comparable rates.

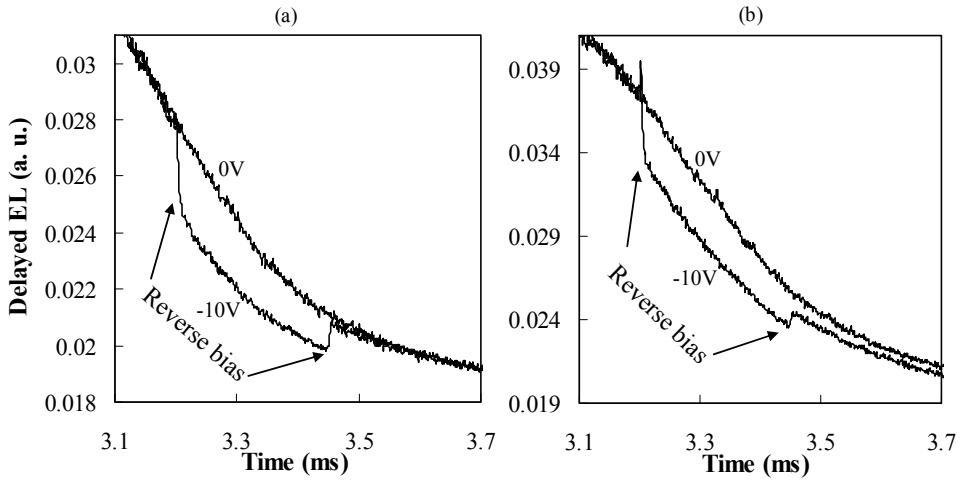


**Figure 4.3: Intensity of delayed EL versus time under forward and reverse bias (a) before and (b) after aging.**

To test if the 535nm emission peak can also be observed in OLEDs where TBADN is doped with a fluorescent guest (which generally demonstrate higher electroluminescence stability in comparison to neat TBADN [47,48,49]), we studied OLEDs of structure ITO/NPB/TBADN:TBP(5%)/$AlQ_3$/Mg:Ag, where TBP is 2,5,8,11-tetra-t-butylperylene. Figure 4.4 depicts delayed EL spectra from this device, collected following 0, 23, 61, 108, 144 and 160 hrs of electrical driving at 30 mA/$cm^2$. In these spectra, the two peaks at 460 nm and 500 nm are the characteristic emission bands of TBP. As can be seen, although at a much slower rate in comparison to the case of neat (undoped) TBADN, devices with TBP-doped TBADN also exhibit peak broadening with electrical aging, which, again, corresponds to an increasing ratio of 535 nm band / TBP emission bands (again, obtained by mathematically subtracting the initial spectrum from the final spectrum), with prolonged electrical stressing.

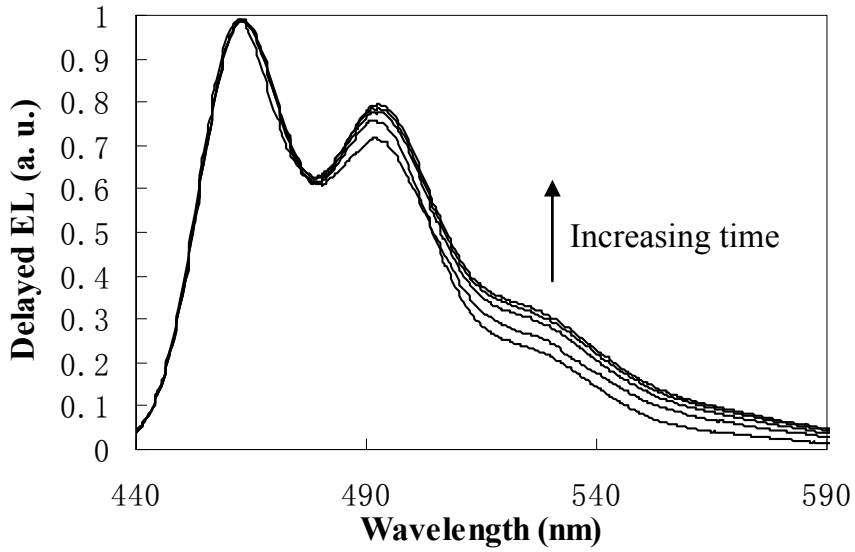


**Figure 4.4: Changes of delayed EL spectra of TBP-doped blue OLED within 160 hours aging.**

Using capacitance measurements, Kondakov *et al* have found a correlation between EL degradation in TBADN-based OLEDs with prolonged electrical stress and the accumulation of trapped charges in the recombination zone, which act as exciton quenchers [30]. Although the underlying mechanisms behind the space charge build-up were not well understood, they observed a strong correlation between the decrease in device luminescence efficiency and the increase in transition voltage for OLED capacitance, an indicator of the amount of trapped charges, which increased continuously with OLED electrical stress time but at an ever-decreasing rate [30]. Discovering here that device efficiency loss is associated with a relative increase in 535 nm emission band arising from the recombination of trapped charges, it is worthwhile finding out if these two phenomena are related. In order to do this, we used the ratio of the intensities of the 535 nm emission to the emitter's singlet emission band in delayed EL spectra as a qualitative indicator of the relative magnitude of recombination of trapped charges with device aging time. Figure 4.5 depicts this ratio for the OLED with TBP (5%)-doped TBADN as a function of aging time, using the 535 nm / 460 nm intensity ratio from the spectra intensities figure 4.4. As showing in the figure, the ratio increases with time at an ever-decreasing rate, following a trend very similar to that observed by Kondakov and co-workers [30]. The close similarity between both results suggests that the species

responsible for the 535nm may itself indeed be responsible for the increased charge trapping with device aging. The much weaker emission from this species in comparison to TBADN emission suggests that it is more efficient in dissipating excitation energy non-radiatively, hence is capable of quenching TBADN singlet excitons, possibly causing the observed efficiency loss with electrical aging.

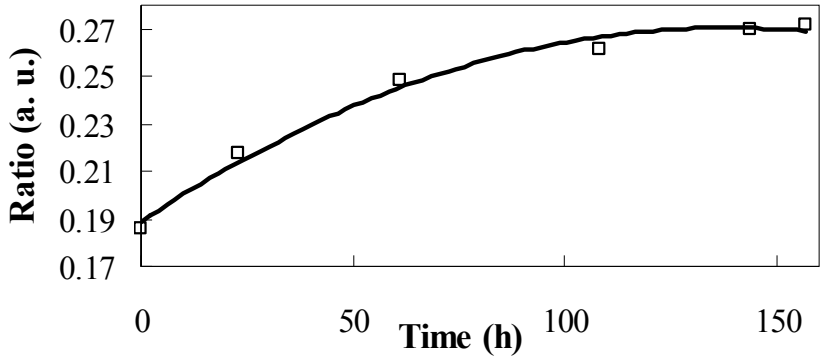


**Figure 4.5: Ratio of 535nm/460nm emission of Figure 4.4.**

Anthracene is known to be prone to molecular aggregation, and dimerization of anthracene derivatives can lead to fluorescence at much longer wavelengths than the monomers, often in the green range [50,51]. In order to investigate if the 535 nm emission can be due to some intermolecular interactions in TBADN, we carried out comparative studies on TBADN and ADN, an anthracene derivative with a molecular structure identical to that of TBADN except that it lacks the bulky tetra butyl group, and therefore is more liable to intermolecular interactions. Figure 4.6 depicts the molecular structure of TBADN and ADN, as well as their absorption and photoluminescence spectra in thin solid films (~100 nm) and diluted solutions ( 0.5% in $CHCl_3$). As evident from the figure, spectra of ADN and TBADN show essentially the same absorption and emission bands, signifying the very similar photophysical properties of both compounds. A comparison of the film versus solution spectra in each case however shows a red shift, and the magnitude of this red shift is significantly larger in case of ADN (~9 nm and ~8 nm for absorption and PL spectra, respectively in case of ADN versus only ~5 nm and ~1 nm for absorption and PL spectra, respectively in case of TBADN). The larger red shift corroborates the

notion of a relatively higher intermolecular interaction in case of ADN thin films. With such knowledge, it is reasonable to expect that ADN based OLEDs would show stronger 535 nm component in EL spectrum than TBADN counterpart. Figure 4.7 shows normalized prompt and delayed EL spectra from electrically un-aged devices of structures ITO/NPB/ADN/$Alq_3$/Mg:Ag and ITO/NPB/TBADN/$Alq_3$/Mg:Ag. Clearly, the device with ADN EML exhibits a much broader prompt EL peak and a stronger 535 nm emission peak in delayed EL spectra. The results indicate that the 535 nm emission in TBADN OLEDs can indeed be due to some intermolecular species associated with increased molecular aggregation. Thermal annealing for 1 hour at 120$^{o}$C is also observed to result in peak broadening in the photoluminescence spectra of ADN thin films (100 nm thick) that again corresponds to increased 535nm/peak emission ratio. This observation not only shows that the effect is based in morphological changes that can, to some extent, be thermally induced, but also reveals that the 535nm emission arising from these intermolecular species likely occurs due to the relaxation of a singlet excited state that can be produced merely by optical excitation. It should be pointed out that unlike ADN, no detectible changes in photoluminescence spectra of thin films of TBADN can be observed after the same thermal annealing treatment, reflecting the higher morphological stability of TBADN.

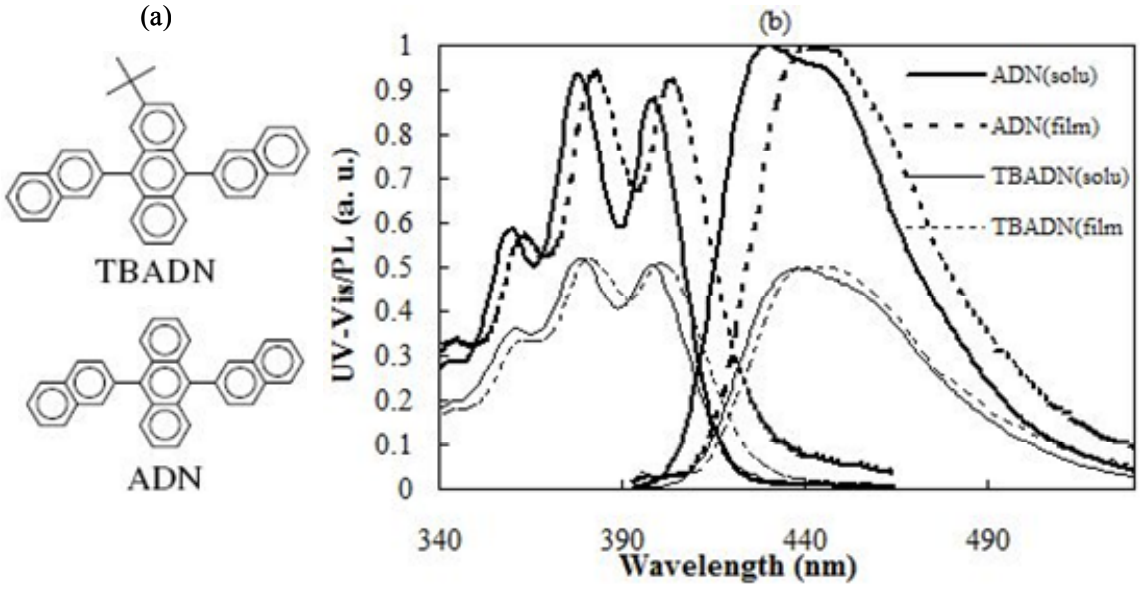


**Figure 4.6: (a) Molecular structure of TBADN and ADN. (b) UV-Vis absorption and PL spectra of TBADN and ADN in films (100nm) and solutions (0.5% in $CHCl_3$).**

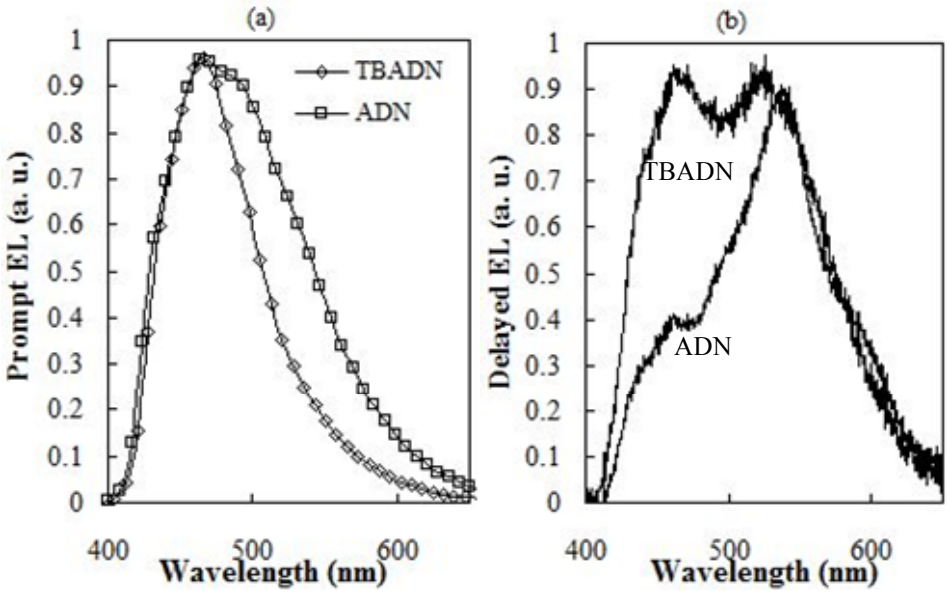


**Figure 4.7: (a) Prompt EL spectra and (b) delayed EL spectra of ITO/NPB/TBADN(ADN)/$Alq_3$/Mg:Ag.**

In order to further investigate the role of molecular aggregation in the 535nm emission component in TBADN OLEDs, we studied OLEDs in which the EML is made of TBADN mixed with 4,4′-N,N′-dicarbazole-biphenyl (CBP). Mixing TBADN with CBP can be expected to interfere with TBADN molecular aggregation process, reducing it on entropy grounds. In the same time, as CBP has a wider energy band gap than TBADN, energy transfer from TBADN to CBP is thermodynamically unfavorable, and so TBADN's role in electroluminescence is maintained. Figure 4.8 shows prompt EL and delayed EL spectra from devices with various concentrations of CBP in the TBADN EML. Clearly, introducing CBP reduces the relative magnitude of the 535 nm emission band in the normalized spectra. The observation that higher CBP concentrations (hence, more diluted TBADN) suppresses the 535 nm emission convincingly proves that the emission arises from some intermolecular TBADN species associated with molecular aggregation. It is noteworthy to point out that the strong dependence of the relative magnitude of 535 nm emission on CBP concentration for values as high as 50% CBP in un-aged devices suggests that molecular aggregation in TBADN can be quite significant even in systems in which TBADN is intermixed with a foreign (guest) material at relatively high concentrations (e.g. 1:1 TBADN:Guest, by volume). This sheds the light on the 535 nm emission observed in the TBADN:TBP

discussed above, and draws the attention to the real possibility of significant molecular aggregation in a wider range of OLEDs in which TBADN is used as a host material for luminescent dopants.

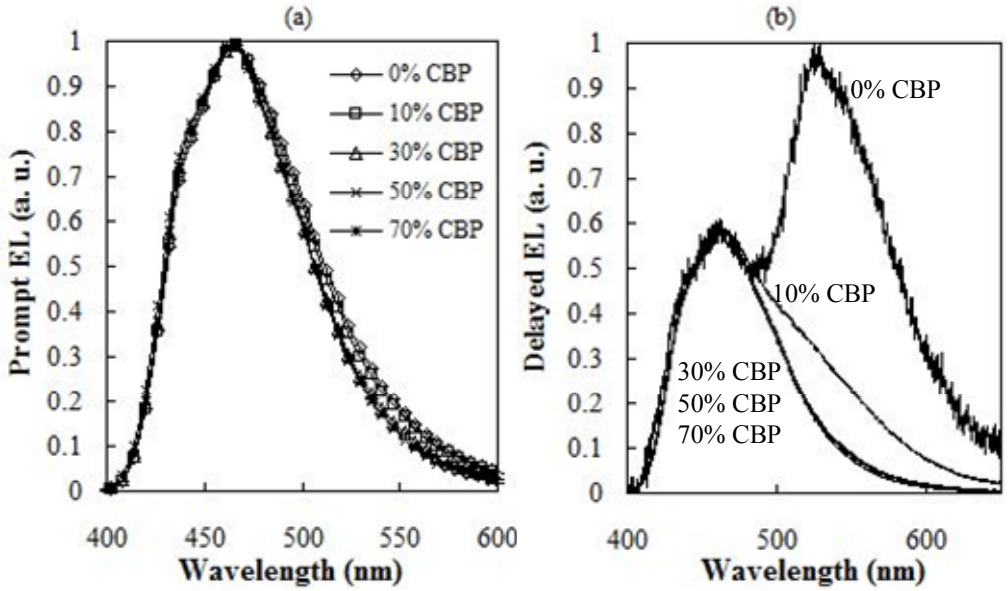


**Figure 4.8: (a) Prompt EL spectra and (b) delayed EL spectra of ITO/NPB/TBADN:CBP/$Alq_3$/Mg:Ag.**

It should be pointed out that although the introduction of a high concentration of CBP substantially reduces the relative magnitude of 535nm emission band in delayed EL spectra, prolonged electrical driving still results in a relative increase in 535nm emission (yet at a slower rate than in neat TBADN OLEDs). This behavior is depicted in figure 4.9. These results suggest that electrical driving can still induce the formation of the green emitting intermolecular species, despite the lower molecular aggregation in the initial morphology. Our studies also show that despite the fact that heating for 1 hour at 120 $^{o}$C does not bring about measurable changes in PL spectra of TBADN, electrical aging brings about detectable changes in PL, even in OLEDs containing CBP intermixed with TBADN (Figure 4.10). As the thermal load of electrical driving is presumably lower, the observation suggests that the increased intermolecular interaction with electrical aging is not simply a crystallization process induced by Joule heating as a result of the current flow. It therefore appears that other factors associated closely linked with electrical driving, such as the formation of exciton and/or polaron intermediates, may be playing a role in the formation of these intermolecular species.

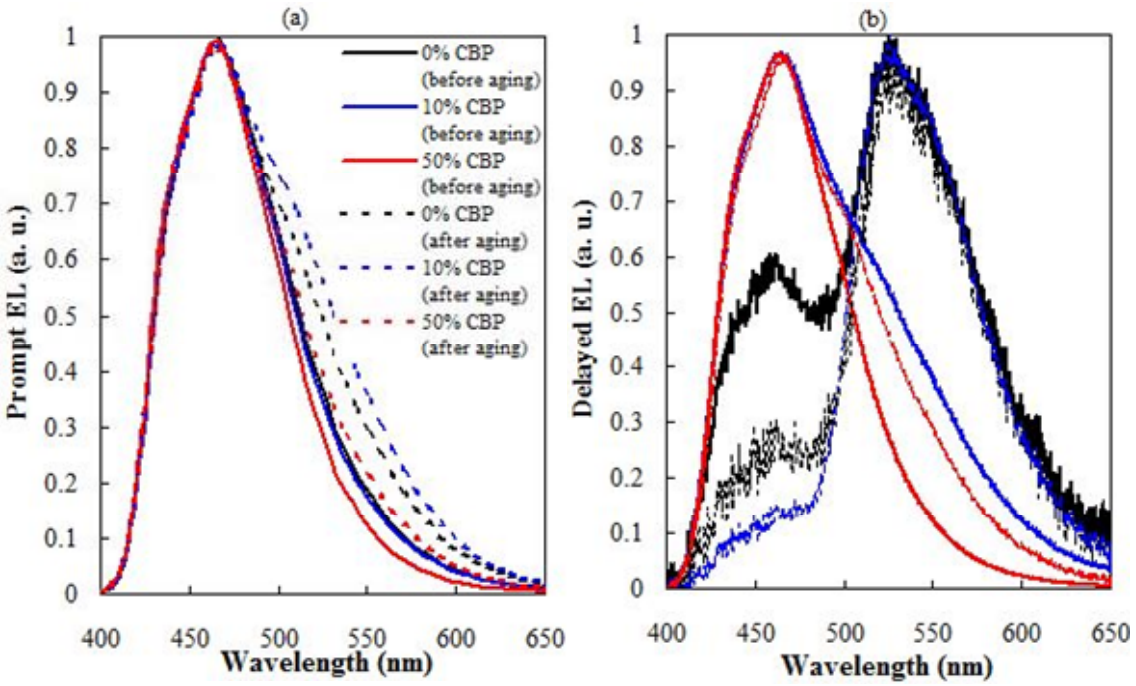


**Figure 4.9: (a) Prompt EL spectra and (b) delayed EL spectra of ITO/NPB/TBADN:CBP/$Alq_3$/Mg:Ag before & after aging**

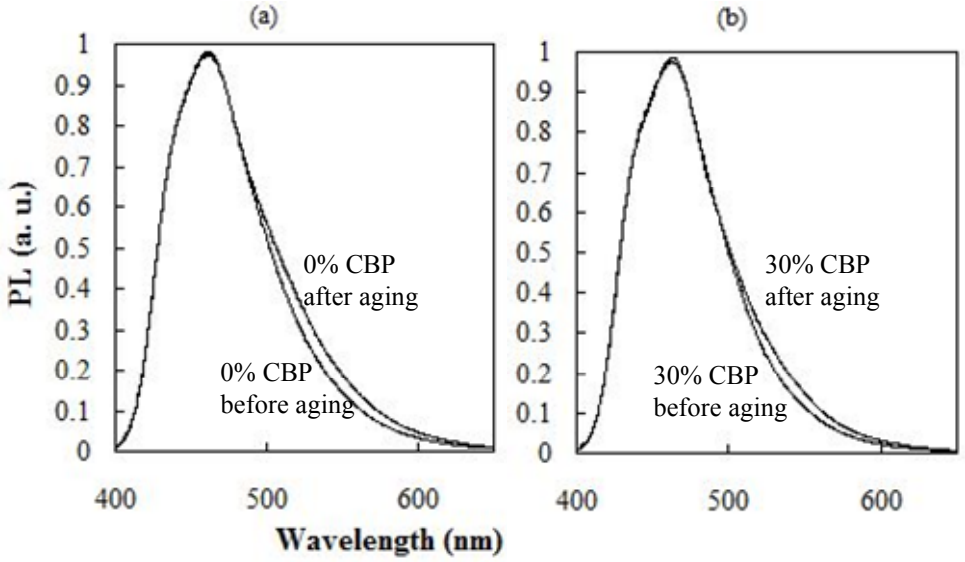


**Figure 4.10: PL spectra of ITO/NPB/TBADN:CBP/$Alq_3$/Mg:Ag before & after aging (100 hrs at 20mA/$cm^2$).**

# Chapter 5

## Photo-degradation of Organic / Metal Cathode Interface in OLEDs[†]

Extensive work has been done to uncover the factors that limit the stability of OLEDs, and several aging mechanisms related to electrical driving [52,53,54,55,56] or exposure to the ambient [57,58,59] have been identified. Contrarily, only very few studies have addressed the question of photo-stability in OLEDs. In these few studies, the investigations have been primarily limited to investigating external factors such as the effect of solar irradiation, or photo-oxidation in the presence of ambient oxygen [60,61,62]. Photo-degradation at optical wavelengths or by device own electroluminescence (EL), a phenomenon that can become increasingly possible as progress in this field continues to make OLEDs more efficient and brighter, has so far been overlooked.

Figure 5.1(a) shows changes in EL (normalized to the initial value at the same current density) and $V_d$ at 0.5 mA/cm$^2$of a blue OLED , versus time elapsed during which the device is subjected to one the following stress scenarios: (i) Stress by light only (denoted by L), during which the OLED is irradiated by 465nm illumination (the wavelength corresponds to the emission peak of TBADN) of power density ~1.2 mW/cm$^2$; (ii) Stress by current only (denoted by I), during which the OLED is under forward bias to sustain a current flow of density ~0.5mA/cm$^2$ ; and (iii) Stress by light and current together (denoted by I+L), during which the OLED is subjected to the conditions of (i) and (ii) simultaneously [32]. The low current density used in scenarios (ii) and (iii), an order of magnitude smaller than currents normally used to operate an OLED at typical EL brightness levels, is chosen in order to ensure that degradation mechanisms arising exclusively from electrical stress remain insignificant [52]. At this low current density, only very weak EL (<10cd/m$^2$) is observed. As can be seen from the figure, subjecting the OLED to light only (scenario i) results in a gradual decrease in its EL efficiency and an increase in its $V_d$,

[†] The main content of this chapter was published in APL [32], and was reproduced here by the permission from AIP.

and these light-induced changes occur more rapidly in the presence of current flow (scenario iii), despite the very low current densities used. On the other hand, changes induced by current flow alone (scenario ii) are relatively much smaller, ascertaining that the changes observed in the other two cases are induced - at least in part - by the presence of light. Figure 5.1(b) presents data from a green OLED subjected to the same stress conditions except that, in this case, the OLED is irradiated by 530nm monochrome illumination (~1.8 $mW/cm^2$) (the wavelength corresponds to the emission peak of $AlQ_3$). As can be seen from figure, the green device shows essentially the same trends, qualitatively, wherein, again, exposure to light (scenario i) brings about changes in its EL efficiency and driving voltage; and the changes are faster in the presence of current (scenario iii). Obviously, the behavior observed in both devices signifies some light-induced degradation processes that result in a deterioration in their EL characteristics. As the changes in EL efficiency and $V_d$ induced by the combination of light and current (scenario iii) are much larger than the sum of those induced by light or current separately, it follows that the flow of current must be playing a role in facilitating this photo-degradation mechanism, suggesting that the underlying processes may be electrochemical in nature. The fact that these processes can be induced by means of illumination of essentially the same wavelengths like that of OLEDs EL indicates that they can, in principle, occur "inherently" by means of device own EL during normal operation. We should point out that this behavior is not limited to irradiating the OLEDs at these specific wavelengths. Irradiating the same OLEDs to other wavelengths such as 370 nm, 405 nm or 440 nm is observed to produce similar trends.

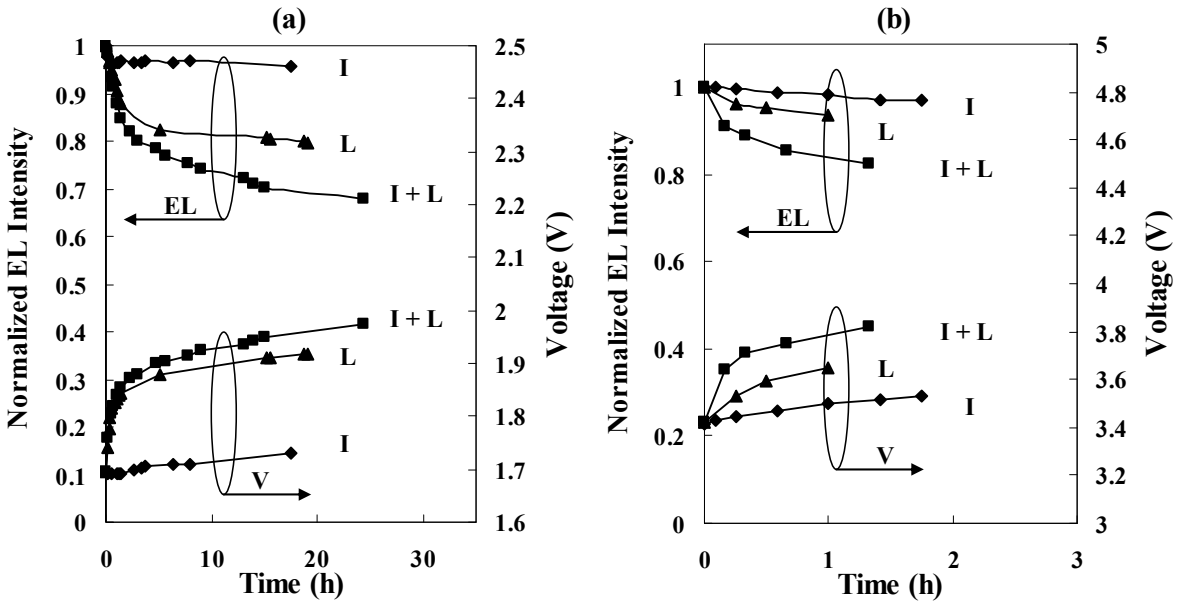


**Figure 5.1: Normalized EL efficiency and $V_d$ at 0.5 mA/cm$^2$ versus stress time for (a) blue OLED and (b) green OLED, under three stress scenarios**

Interestingly, we found out that the light-induced changes can be eradicated by removing the metal cathode, and depositing a new one on the same organic stack. Figure 5.2(a) illustrates this effect in case of a blue OLED with a Mg:Ag cathode. The photograph on the left shows EL from the OLED at 20 μA/cm$^2$ after exposure to 465 nm illumination in the presence of current flow for about 2 hours. In this device, a masking tape is used to cover one half of the device area (corresponds to the right half in the photograph), shielding it from the light. As such, the left half is subjected to both light and current (scenario iii) whereas the right half is subjected to current only (scenario ii). As can be seen from the photograph, the brightness of the left half (i.e. the irradiated half) is much lower, reflecting the photo-degradation effect. Photoluminescence tests show that despite their different EL intensities, both areas give essentially the same fluorescence intensity, suggesting that the lower EL from the irradiated area is not due to changes in the bulk of the emitter material, as may result from photo-oxidation [61] or the formation of quenchers [30]. The photograph on the right shows EL from the same device after its cathode has been removed (by peeling it off using scotch tape [60]), and a new one, also Mg:Ag, is deposited. As the photograph clearly shows, replacing the cathode causes the difference in brightness to

disappear, making emission from the entire device uniform. Measurements show that replacing the cathode causes EL and $V_d$ to recover, in this case almost completely, to their original (i.e. pre-irradiation) values. These results convincingly show that the observed photo-degradation behavior must be due to changes in the metal cathode or at the cathode / organic interface that cause electron injection to become more difficult, hence the increase in $V_d$. The recovery in EL confirms that its earlier decrease is indeed not due to a decrease in the fluorescence quantum yield of the emitter material [52] or the diffusion of metal ions into the organic layers [63]; rather the result of changes in charge balance caused by the deteriorating electron injection. In view of these findings, it is imperative to question if the observed effect is limited to $AlQ_3$/ Mg:Ag contact, or if it can occur in other cathode contact materials. We therefore test OLEDs with LiF/Al cathodes and/or BAlQ ETL. Figure 5.2(b) shows results from the same experiment carried out on a blue OLED with a LiF/Al cathode (instead of Mg:Ag). As before, areas irradiated by 465nm illumination (left photograph, left half) display lower EL brightness versus non-irradiated areas (left photograph, right half), showing that the same photo-degradation mechanism also occurs in devices with LiF/Al cathode. As before, removing the LiF/Al and depositing a new one makes emission from the entire device uniform (right photograph), again showing that the photo-degradation is associated with the cathode contact. In this case, however, the recovery of EL and $V_d$ upon replacing the LiF/Al cathode with a new one is found to be only partial. The partial recovery in this case may be due to the stronger contact adhesion [64] which can cause more residual material from the first cathode to remain on the ETM, undermining the quality of the new contact. Studies on OLEDs utilizing BAlQ instead of $AlQ_3$ as ETL also reveal the same behavior. These findings therefore show that the photo-degradation of the metal/organic contact can indeed be a phenomenon of wider presence in OLEDs.

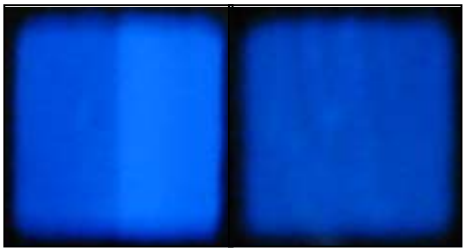

**(a) Mg:Ag as Cathode**

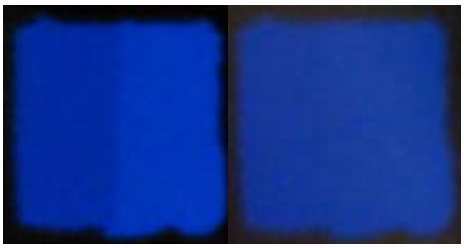

**(b) LiF/Al as Cathode**

**Figure 5.2: Photographs showing EL from blue OLEDs with (a) Mg:Ag cathode , and (b) LiF/Al cathode, that have been partially exposed to external illumination**

To verify if the light-induced changes in $V_d$ and EL efficiency are indeed due to a deterioration in electron injection at the cathode contact, we study blue emitting devices that include a "marking layer", inserted between the NPB and TBADN layers, containing 4-(dicyanomethylene)-2-t-butyl-6-(1,1,7,7-tetramethyljulolidyl-9-enyl)-4H-pyran (DCJTB) red emitting dopant (2%). The device structure is ITO/NPB(40nm)/TBADN:DCJTB(5nm)/TBADN(40nm)/$AlQ_3$(20nm)/Mg:Ag. EL spectral measurements on this device show emission from both DCJTB and TBADN (reflected in the 595nm peak and the 465nm shoulder, respectively), with DCJTB emission being much stronger (Figure 3.13) due to the close proximity of the marking layer to the electron-hole recombination zone [52]. Figure 5.3 shows EL spectra collected from this device before and after exposure to 465 nm irradiation in the presence of current flow (0.5 mA/cm$^2$) (scenario iii) for a period of about two hours. During this time, the DCJTB peak decreases by ~20% while that of TBADN decreases by only ~12%. The different rates of decrease of the two peaks indicate a change in the ratio of photons emitted from the two materials, revealing a

gradual shift of the recombination zone towards the cathode, consistent with a deteriorating electron injection at the metal cathode. The results therefore show that the light-induced changes in $V_d$ and EL (in Fig. 5.1) are indeed associated with a deterioration in electron injection, which expectedly can alter charge balance.

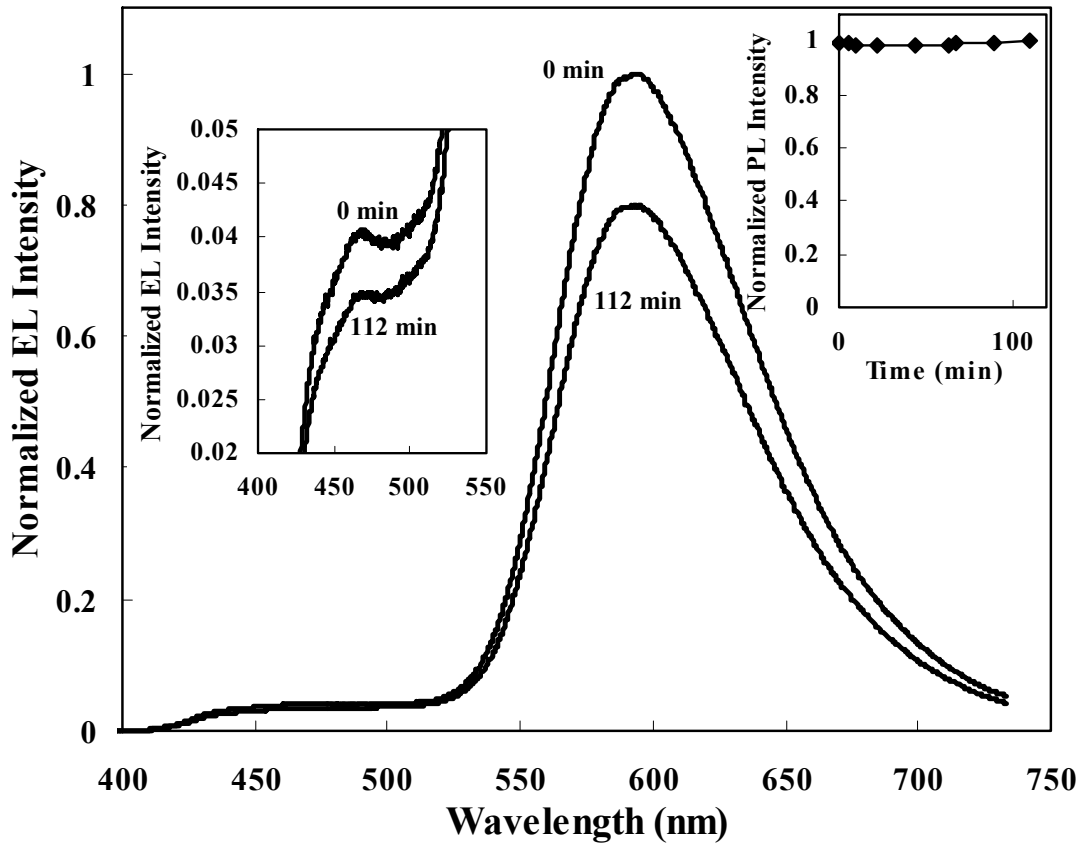


**Figure 5.3: EL spectra of device of structure ITO/NPB(40nm)/TBADN:DCJTB(5nm)/TBADN(40nm)/$AlQ_3$(20nm)/Mg:Ag before and after being subjected to stress scenario (iii) for a period of 112 min.**

Finding that the organic/cathode contact of an OLED is susceptible to photo-degradation, especially in the presence of current flow, and that the phenomenon can be induced by illumination of wavelengths similar to those of device EL emission, it becomes interesting to find out if the same phenomenon may indeed be occurring "inherently" during device normal operation, without the external illumination, and if

it contributes to their known electrical aging behavior [52]. The typically high OLED EL powers (usually > 100 mW/cm$^2$), combined with the relatively high currents (usually > 10 mA/cm$^2$) normally used to drive them suggest that the phenomenon can occur readily. To test for evidence for this phenomenon, we study the effect of replacing the cathode of a green OLED after several hours of operation at an average current density of 60 mA/cm$^2$ using ac driving mode. At this current, the initial luminance and voltage are 1200 cd/m$^2$ and 7.48 V, respectively. After about 30 hours of driving, the cathode is removed and a new one is deposited, and driving at the same current is resumed. Figure 5.4 shows changes in EL efficiency and $V_d$ versus driving time of this OLED with the original cathode, and also after the cathode is replaced. As can be seen from the figure, the prolonged electrical driving brings about a gradual decrease in EL efficiency and increase in $V_d$, as commonly seen in OLEDs [52]. Replacing the cathode, on the other hand, leads to an abrupt recovery in both properties, eradicating the majority of the preceding changes, leaving only a small residual (i.e. permanent) change in their values (versus their initial values at time zero). Obviously, such recovery in EL and $V_d$ on replacing the cathode reveals that the changes they display during the preceding 30 hours of electrical driving are caused primarily by a deterioration of the organic/metal contact, suggesting that the same photo-degradation mechanism can indeed be occurring, inherently, by device own EL. It should be pointed out that simply "resting" a device after it has been exposed to these electrical stresses, by leaving it without electrical bias for several hours, does not bring about a recovery in EL and $V_d$, indicating that the recovery is not primarily due to the slow relaxation of space charges [46]. We should also point out that replacing the cathode after longer periods of operation often leads to a smaller recovery in EL and $V_d$ , signifying a larger permanent change component. This permanent change, which can not be eliminated by replacing the cathode, is indicative of the presence of additional degradation mechanisms, not associated with the cathode contact whose effects become increasingly significant when OLEDs are driven for much longer periods of time [52]. Similar investigations of blue OLEDs reveal the same effects. These results suggest that inherent photo-degradation of the organic / metal cathode can indeed be playing a significant role in limiting the stability of OLEDs.

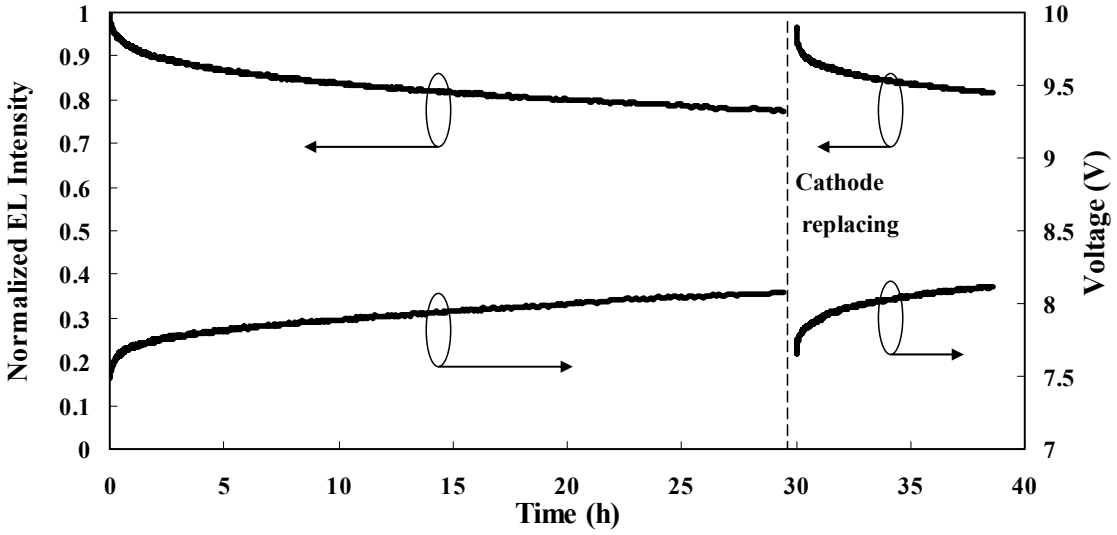


**Figure 5.4: Normalized EL efficiency and $V_d$ versus driving time at 60mA/cm$^2$ in case of a green device with Mg:Ag cathode. After almost 30 hours of driving, cathode is replaced, and driving is resumed.**

# Chapter 6

# Summary, Conclusions and Future Work

## 6.1 Summary and Conclusions

In summary, electrical aging in anthracene-based OLEDs is found to be associated with an increasing concentration of an intermolecular species with a weak characteristic luminescence around 535 nm. Although the exact nature of this species is not fully understood, the results suggest it may be the product of molecular dimerization or some chemical and morphological changes in TBADN facilitated by anionic or cationic TBADN intermediates. This species is capable of charge trapping, and thus plays a role as an electron-hole recombination center with prolonged electrical driving. Weak green luminescence from this species leads to an increased green/blue emission ratio, and causes the color purity loss in aged devices. The results also suggest that this species is also efficient in dissipating excitation energy non-radiatively, hence is capable of quenching TBADN singlet excitons, contributing to the observed efficiency loss with electrical aging. Although increased molecular aggregation and smaller intermolecular distance are key factors in the formation of this species, the increase in its concentration with prolonged OLED electrical driving appears to be primarily due to processes closely related to electrical driving (electro- and/or photo- physical or chemical processes), rather than being simply the result of Joule heating by the current flow.

Also, it is found that the organic/cathode contact of an OLED is susceptible to photo-degradation, especially in the presence of current flow. This photo-degradation can occur inherently in the devices during their normal operation. The results uncover an important degradation mechanism in OLEDs and shed the light on a phenomenon that is expected to be playing a role in limiting the stability of other organic optoelectronic and photovoltaic devices such as photo-detectors and solar cells.

## 6.2 Future Work

Electrical aging in anthracene-based OLEDs is found to cause the formation of an intermolecular species whose luminescent peak is at around 535nm, possibly the dimer or aggregate of anthracene derivatives. So far such formation of molecular aggregate induced by electrical aging has been only observed in anthracene-based OLEDs. It may be possible that the same process takes place in other commonly used light emitting molecules such as $AlQ_3$ or $Ir(ppy)_3$ but only the emerging peak is near infrared region so that the molecular aggregation is not affecting the color purity during electrical aging. However, after all the molecular aggregation is not in favor of quantum efficiency because a group of molecules together act as an inefficient light emitting entity instead of one. Thus, it may be interesting to investigate the electrical aging induced molecular aggregation in other types of OLEDs by using infrared spectrometer.

As concluded in chapter four, the nature of the formation mechanism of such molecular aggregate is not clear, and Joule heating is not responsible for its formation. Moreover, other factors such as prolonged current flowing or optical irradiation do not result in the formation of the molecular aggregation independently either. The production mechanism of the molecular aggregation may involve very complicated physical/chemical processes in which more than two factors together influence on the molecular characteristics. One straightforward approach to uncover the question is to study the polaron-exciton interaction, in which electron/hole only current devices with TBADN as active layer are subjected to prolonged optical excitation from a UV lamp and electrical stress current simultaneously. However, preliminary study does not show the change of the PL of TBADN after enough long stress time. This result still cannot rule out the effect of polaron-exciton interaction on the formation of molecular aggregation because the concentration of exciton created optically by a UV lamp is far lower than that created electrically by charge injection in operating OLEDs. Therefore, it is meaningful to further study such effect by using a laser instead of a UV lamp, which could create tremendous excitons optically.

It should be pointed out that the optically created excitons are nearly pure singlet excited states, but in normal operating OLEDs the main accumulation of excitons is the triplet excited states in that three times higher amount of triplets are created and long-lived (the lifetime of triplet is typically five to six

orders of magnitude longer than that of singlet in fluorescent OLEDs) compared to singlets. Also, as commonly observed in all types of OLEDs, the bimolecular process TTA cannot be overlooked in the investigation of molecular aggregation here. So the polaron-triplet interaction (not the above polaron-singlet interaction) might cause the molecular aggregation, although such interaction is difficult to be investigated directly since triplets are not easy to be generated optically. Thus, another possible approach could be studying the correlation between the amount of accumulated triplets and the molecular aggregation in operating OLEDs. To accomplish this, a triplet scavenger, a guest molecule whose triplet energy gap is smaller and singlet energy gap is larger than the host molecule, is needed to be doped into TBADN in order to scavenge the TBADN triplets but keep singlets [65,66,67]. Correspondingly, delayed EL measurement can be used to quantitatively reflect the amount of triplets. Unfortunately, so far no suitable triplet scavenger that can be thermally evaporated has been developed and synthesized for anthracene-based OLEDs.

Although the formation mechanism of molecular aggregation is not well understood, the issue of color purity loss with electrical aging still can be partially solved by introducing molecular spacers such as CBP into functional molecules to decrease the intermolecular interactions, used in chapter four. But the disadvantage of this method is obvious, i.e. the lower EL efficiency due to the introduction of molecular spacer. A permanent solution might be accomplished through the engineering of molecular structure in which a much larger bulky side group is added onto the anthracene core to increase the intermolecular distance and reduce the aggregation tendency.

On the other hand, besides the intrinsic molecular degradation of the bulky organic light emitting material, the photo-degradation of the organic/metal electrode interface is also playing a very important role in limiting the device stability. As concluded in chapter five, the photo-degradation can occur inherently in the devices during their normal operation, resulting in the deterioration of electron injection from the cathode and thus the reducing the EL efficiency. However, the photo-degradation mechanism at the organic/metal electrode needs to be further investigated.

One possible photo-degradation mechanism may be that new metal oxide is created at the organic/cathode interface by photo-oxidation and such metal oxide layer acts as an electron blocking

layer between ETL and cathode. In order to make sure if new metal oxide is created after photo-degradation, X-ray photoelectron spectroscopy (XPS) is required to measure the chemical composition that exists within the device, especially near the ETL/cathode interface. Also, another possible photo-degradation mechanism may be the delamination between ETL and cathode that results in the difficulty in electron injection. Atom force microscope (AFM) can be used to study the change of surface roughness of either organic layer or cathode layer before and after photo-degradation.

In addition to focusing on the direct chemical/physical change of the organic/metal electrode interface induced by photo-degradation, a distinctive dimension to explore the photo-degradation mechanism is through studying the correlation between the ETL absorption spectrum and rate of photo-degradation at different optical excitation wavelength. That is to say, the rate of the photo-degradation of the organic/metal electrode interface at certain excitation wavelength might be strongly dependent on the absorption ability of organic layer at the same excitation wavelength. This requires a systematic study on the rates of photo-degradation at different excitation wavelengths, and one potential difficulty is that most of Hg-Xe lamps that used as irradiation source do not have a uniform optical output.

It should be mentioned that once the optical excitation wavelength goes below 400nm in the study the photo-degradation of the anode/organic interface cannot be neglected because NPB, as a HTL, is efficiently excited below 400nm. As a matter of fact, such photo-degradation of the ITO/NPB interface is indeed observed indirectly in our preliminary study.

Now with the knowledge and the experience from the latest study on the photo-degradation of the organic/metal electrode interface of OLEDs, a solution to the photo-degradation is proposed and applied in practice. The recent study in our group shows that the photo-degradation is greatly reduced and the device stability is dramatically improved by inserting a $Cs_2CO_3$ buffer layer between organic ETL and metal cathode, although the fundamental mechanism for such improvement is not clearly confirmed [68,69,70,71,72]. Moreover, some other compounds and oxides may also be effective in improving the photo-stability of device when inserted between the ETL and cathode [73,74,75,76,77], and their availabilities are needed to be further verified.

Finally, all the scientific progress related to the photo-degradation and its solution in OLEDs can be seriously considered and applied in other organic optoelectronic and photovoltaic devices such as photo-detectors and solar cells, because these optoelectronic devices are continuously exposed to light at different wavelengths and the photo-degradation might be even more predominant in limiting the overall device stability.

# Bibliography


1 Photographs are adapted from http://en.wikipedia.org.

2 A. Bernanose, M. Comte, P. Vouaux, J. Chim. Phys. 50, 64 (1953).

3 E. Gurnee, R. Fernandez, U.S. Patent 3,172,862.

4 B. A. Bolto, R. McNeill, D. E. Weiss, Aus. J. Chem. 16, 1090 (1963).

5 H. Shirakawa, E. J. Louis, A. G. MacDiarmid, C. K. Chiang and A. J. Heeger, J. Chem. Soc., Chem. Commun. 578 (1977).

6 R. H. Partridge, Polymer 24, 733, 739, 748, 755 (1983).

7 C. W. Tang, S. A. VanSlyke, Appl. Phys. Lett. 51, 913 (1987).

8 T. R Hebner, C. C. Wu, D. Marcy, M. H. Lu, J. C. Sturm, Appl. Phys. Lett.72, 519 (1998).

9 W. Schottky, Phys. Z. 41, 570 (1940).

10 Physics of Organic Semiconductors, edited by W. Brutting, WILEY-VCH Verlag GmbH & Co. KGaA, Weinheim, 2005.

11 H. Ishii, K. Sugiyama, E. Ito, and K. Seki, Adv. Mater. 11, 605 (1999).

12 W. Brutting, ICEL2 Tutorial on OLEDs.

13 K.P.C. Vollhardt, Organische Chemie, VCH-Verlag, Weinheim 1990.

14 H. Bassler, phys. stat. sol. (b) 107, 9 (1981).

15 Adapted from http://www.mineralienatlas.de.

16 C. W. Tang and S. A. VanSlyke, Appl. Phys. Lett. 51, 913-915 (1987).

17 J. H. Burroughes, D. D. C. Bradley, A. R. Brown, R. N. Marks, K. Mackay, R. H. Friend, P. L. Burns, and A. B. Holms, Nature 347, 539-541 (1990).

18 H. Aziz, Z. D. Popovic, N.-X. Hu, A.-M. Hor, and G. Xu, Scince 283, 1900 (1999).

19 Y. Z. Wu, X. Y. Zheng, W. Q. Zhu, R. G. Sun, X. Y. Jiang, Z. L. Zhang, and S. H. Xu, Appl. Phys. Lett. 83, 5077 (2003).

20 Y. Kim, E. Oh, D. Choi, H Lim, and C.-S. Ha, Nanotechnology 15, 149-153 (2004).

21 S. W. Culligan, A. C.-A. Chen, J. U. Wallace, K. P. Klubek, C. W. Tang,and S. H. Chen, Adv. Funct. Mater. 16, 1481 (2006).

22 S. Y. Ni, X. R. Wang, Y. Z. Wu, H. Y. Chen, W. Q. Zhu, X. Y. Jiang, and Z. L. Zhang, Appl. Phys. Lett. 85, 6 (2004).

23 J. Shi and C. W. Tang, Appl. Phys. Lett. 80, 3201 (2002).

24 S. Tao, Z. Hong, Z. Peng, W. Ju, X. Zhang, P. Wang, S. Wu, S. Lee, Chem. Phys. Lett. 397, 1-4 (2004).

25 Y. Li, M. K. Fung, Z.Xie, S. T. Lee, L. S. Hung, and J. Shi, Adv. Func. Mater. 14, 18 (2002).

26 X. Y. Jiang, Z. L. Zhang, X. Y. Zheng, Y. Z. Wu, and S. H. Xu, Thin Solid Films 401, 251 (2001).

27 Y. H. Kim, D.C. Shin, S. H. Kim, C. H. Ko, H. S. Yu, Y. S. Chae, and S. K. Kwon, Adv. mater. 13, 22 (2001).

28 K. Danel, T. H. Huang, J. T. Lin, Y. T. Tao, and C. H. Chuen, Chem. Mater. 14, 3860 (2002).

29 M. Pope, H. P. Kallmann, and P. Magnante, J. Chem. Phys. 38,2042-2043 (1963).

30 D. Y. Kondakov, J. R. Sandifer, and C. W. Tang, J. Appl. Phys. 93, 1108-1119 (2003).

31 D. Y. Kondakov, J Appl. Phys. 97, 024503 (2005).

32 Q. Wang, Y. Luo, and H. Aziz, Appl. Phys. Lett. 97, 063309 (2010).

33 Z. D. Popovic and H. Aziz, J. Appl. Phys. 98, 013510 (2005).

34 Y. Luo and H. Aziz, Adv. Funct. Mater. 20, 1285 (2010).

35 W. Staroske, M. Pfeiffer, K. Leo, and M. Hoffmann, Phys. Rev. Lett. 98, 197402 (2007).

36 V. V. Jarikov and D. Y. Kondakov, J. Appl. Phys. 105, 034905 (2009).

37 J.-R. Gong, L.-J. Wang, S.-B. Lei, C.-L. Bai, X.-H. Zhang, and S.-T. Lee, J. Phys. Chem. 109, 1675-1682 (2005).

38 S. A. Vanslyke, C. H. Chen, and C. W. Tang, Appl. Phys. Lett. 69, 2160-2162 (1996).

39 Q. Wang, Y. Luo, and H. Aziz, J. Appl. Phys. 107, 084506 (2010).

40 T. Sadek, H. Aziz, R. O. Loutfy, and P. M. Smith, Proceedings of the IEEE Canadian Conference on Electrical and Computer Engineering, Niagara Falls, Ontario, May 2008, pp 1064–1067.

41 D. Y. Kondakov, J. Appl. Phys. 102, 114504 (2007).

42 Y. Luo, and H. Aziz, Appl. Phys. Lett. 95, 073304 (2009)

43 R. G. Kepler, J. C. Caris, P. Aviakan, and E. Abramson, Phys. Rev. Lett. 10, 400 (1963).

44 B. Yang, S.-K. Kim, H. Xu, Y. Park, H. Zhang, C. Gu, F. Shen, C. Wang, D. Liu, X. Liu, M. Hanif, S. Tang, W. Li, F. Li, J. Shen, J.-W. Park, and Y. Ma, Chem. Phys. Chem. 9, 2601-2609 (2008).

45 C. Ganzorig and M. Fujihira, Appl. Phys. Lett. 81, 3137 (2002).

46 T. Tsujioka, Y. Hamada, and H. Takahashi, Jpn. J. Appl. Phys. Part 1 39, 3463 (2000).

47 V. V. Jarikov, R. H. Young, J. R. Vargas, C. T. Brown, K.. P. Klubek, and L. S. Liao, J. Appl. Phys. 100, 094907 (2006).

48 V. V. Jarikov, J Appl. Phys. 100, 014901 (2006).

49 V. V. Jarikov, Appl. Phys. Lett. 92, 244103 (2008).

50 E. A. Chandross, J. Chem. Phys. 43, 4175 (1965).

51 E. A. Chandross and J. Ferguson, J. Chem. Phys. 45, 397 (1966).

52 H. Aziz and Z. D. Popovic, Chem. Mater. 16, 4522 (2004).

53 R. Meerheim, K. Walzer, M. Pfeiffer, and K. Leo, Appl. Phys. Lett. 89, 061111 (2006).

54 D. Y. Kondakov, W. C. Lenhart, and W. F. Nichols, J. Appl. Phys. 101, 024512 (2007).

55 N. C. Giebink, B. W. D'Andrade, M. S. Weaver, J. J. Brown, and S. R. Forrest, J. Appl. Phys. 105, 124514 (2009).

56 C. Fery, B. Racine, D. Vaufrey, H. Doyeux, and S. Cina, Appl. Phys. Lett. 87, 213502 (2005).

57 H. Aziz, Z. Popovic, C. P. Tripp, N. Hu, A. Hor, and G. Xu, Appl. Phys. Lett. 72, 2642 (1998).

58 H. Aziz, Z. Popovic, S. Xie, C. P. Tripp, N. Hu, A. Hor, and G. Xu, Appl. Phys. Lett. 72, 756-758 (1998).

59 Y. Liew, H. Aziz, N. Hu, H. Chan, G. Xu and Z. Popovic, Appl. Phys. Lett. 77, 2650 (2000).

60 H. Heil, G. Andress, R. Schmechel, H. von Seggern J. Steiger K. Bonrad and R. Sprengard, J. Appl. Phys. 97, 124501 (2005).

61 S. Scholz, C. Corten, K. Walzer, D. Kuckling, and K. Leo, Org. Electron. 8, 709-717 (2007).

62 M. O. Reese, A. J. Morfa, M. S. White, N. Kopidakis, S. E. Shanheen, G.Rumbles, and D. S. Ginley, Sol. Energy Mater. Sol. Cells 92, 746-752 (2008).

63 Ta-Ya Chu, Yong-Han Lee, and Ok-Keun Song, Appl. Phys. Lett. 91, 223509 (2007).

64 T. Tong, B. Babatope, S. Admassie, J. Meng, O. Akwogu, W. Akande, and W. O. Soboyejo, J. Appl. Phys. 106, 083708 (2009).

65 S. Schols, A. Kadashchuk, P. Heremans, A. Helfer, and U. Scherf, Chem. Phys. Chem. 10, 1071 (2009).

66 V. G. Kozlov, V. Bulovic, P. E. Burrows, M. Baldo, V. B. Khalfin, G. Parthasarathy, S. R. Forrest, Y. You, M. E. Thompson, J. Appl. Phys. 84, 4096 (1998).

67 V. I. Adamovich, S. R. Cordero, P. I. Djurovich, A. Tamayo, M. E. Thompson, B. W. D'Andrade, S. R. Forrest, Org. Electron. 4, 77 (2003).

68 L. S. Hung, C. W. Tang, and M. G. Mason, Appl. Phys. Lett. 70, 13 (1997).

69 H. Heil, J. Steiger, S. Karg, M. Gastel, H. Ortner, and H. von Seggern, J Appl. Phys. 89, 1 (2001).

70 C. Wu,C. Lin, Y. Chen, M. Chen,Y. Lu and C. Wu, Appl. Phys. Lett. 88, 152104 (2006).

71 Y. Li, D. Zhang, L. Duan, R. Zhang, L. Wang, and Y. Qiu, Appl. Phys. Lett. 90, 012119 (2007).

72 J. Huang, Z. Xu, and Y. Yang, Adv. Funct. Mater. 17, 1966 (2007).

73 G. E. Jabbour, B. Kippelen, N. R. Armstrong, and N. Peyghambarian, Appl. Phys. Lett. 73, 9 (1998).

74 S. J. Kang, D. S. Park, S. Y. Kim, C. N. Whang, K. Jeong, and S. Im, Appl. Phys. Lett. 81, 14 (2002).

75 Y. Yi, Seong J. Kang, K.Cho, J. Koo, K. Han, K. Park, M. Noh, C. Whang, and K. Jeong, Appl. Phys. Lett. 86, 213502 (2005).

76 J. Lee and Y. Park, Appl. Phys. Lett. 80, 17 (2002).

77 A. Gassmann, C. Melzer, and H. von Seggern, J Appl. Phys. 105, 084513 (2009).